

Triple junction polymer solar cells

Cite this: *Energy Environ. Sci.*, 2013, **6**, 3150

Olusegun Adebajo,^a Purna P. Maharjan,^a Prajwal Adhikary,^a Mingtai Wang,^b Shangfeng Yang^c and Qiquan Qiao^{*a}

Similar to single and double junction polymer solar cells, triple junction devices can also be fabricated from all-solution processing. Although single and double junction polymer solar cells have exhibited an efficiency of 11.1% and 10.6% respectively, the triple junction structure shows promise in significantly increasing the device efficiency. In this work, the efficiency prediction for triple junction polymer solar cells and their dependence on subcell bandgaps, cutoff absorption wavelengths and active layer thicknesses are calculated and reviewed. Recent developments of triple junction polymer solar cells including intermediate layer materials, device performance evolution and future direction are presented. Also low bandgap polymers that are currently used or can potentially be used in triple junction solar cells are reviewed. This review provides researchers with a deep understanding and guidance in developing high performance triple junction polymer solar cells.

Received 4th July 2013

Accepted 27th August 2013

DOI: 10.1039/c3ee42257g

www.rsc.org/ees

Broader context

Current energy consumption is dominated by fossil fuels that are limited, expensive and can pollute the environment. There is therefore a rational need to scale up complementary energy sources and technologies that are abundant, economical and environmentally attractive. Among potential energy sources, the energy resource from the sun is unrivalled. Existing technologies that utilize the abundant solar energy are still cost prohibitive. Emerging solar cell technologies using polymeric materials offer potentially lower cost, lightweight materials, processing ease and large-area manufacturing. Polymer solar cells however still suffer from low efficiency. Significant progress has been made on improvement of the reported efficiencies; however, this progress still needs further improvement for polymer solar cells to compete favourably with the existing technologies dominating the market. While the performance of single junction polymer solar cells is limited due to various unavoidable energy losses, multijunction polymer solar cells involving the stacking together of two or more single junctions with complementary absorption are viable alternatives for circumventing the limitations of single junction cells. This review insightfully addresses various important issues that help in the understanding of the device operation and advance the efficiency of triple junction polymer solar cells.

1. Introduction

Organic photovoltaics (OPVs) based on π -conjugated molecular materials have been attracting growing academic and industrial interest in the last few decades largely due to the inevitable need to find cost effective, abundant, sustainable, clean, and ubiquitous alternatives to conventional fossil fuel energy sources.^{1–3} Solar cells based on silicon (Si) and other inorganic compound materials dominating the current photovoltaic (PV) market are expensive due to high manufacturing and material cost;^{4,5} however, the recent cost drop in Si solar cells makes the PV technology more and more promising in the energy market. Development of OPVs is driven by their prospect of low cost, high throughput and large scale manufacturing *via* printing,

spraying or solution casting.^{6–8} In addition, OPVs are light-weight, mechanically flexible and have great potential to be integrated into buildings.⁹ The chemical structures of OPV materials (*e.g.* polymers, oligomers and small molecules) can also be easily engineered to achieve desired optical and electronic properties including low bandgaps, controllable energy levels and high carrier mobilities.

In the pioneering work by Tang a bilayer heterojunction device structure comprising of two different organic semiconductors was used and an efficiency of $\sim 1\%$ was achieved in the 1980s.¹⁰ The role of a heterojunction is to separate photo-generated excitons. However, this bilayer approach was limited by the short exciton diffusion length and inefficient donor–acceptor interfacial area. Early demonstration of bulk heterojunctions made by using a mixture of two polymers¹¹ or a polymer and a soluble fullerene molecule was successful with the promise of high efficiency in charge separation and generation.¹² This led to tremendous advances in the study of bulk heterojunction (BHJ) OPVs. Though the BHJ concept can improve the donor–acceptor interfacial area and shorten the distance over which excitons have to diffuse, critical issues still exist. For example, isolated and/or disordered molecular

^aCenter for Advanced Photovoltaics, Department of Electrical Engineering and Computer Sciences, South Dakota State University, Brookings, SD, 57007, USA. E-mail: Qiquan.Qiao@sdstate.edu; Fax: +1-605-688-4401; Tel: +1-605-688-6965

^bInstitute of Plasma Physics, Chinese Academy of Sciences, Hefei 230031, PR China
^cHefei National Laboratory for Physical Sciences at Microscale, CAS Key Laboratory of Materials for Energy Conversion & Department of Materials Science and Engineering, University of Science and Technology of China (USTC), Hefei 230026, PR China

packing may act as charge traps resulting in low mobilities.² This requires a bicontinuous interpenetrating network of donor and acceptor phases through the medium.^{13,14} As reported by Darling *et al.*, the OPV performance also depends on various factors such as crystallinity, phase-separated morphology, molecular stacking, and relative miscibility of the components.^{15,16}

To achieve high efficiency OPVs, a substantial amount of light needs to be absorbed in active materials. This requires an active layer film with enough thickness and broad spectrum absorption. However, the low carrier mobility associated with disordered organic materials favors a thin film for efficient charge transport. Therefore, a trade-off thickness of the photoactive layer that supports both light harvesting and charge transport needs to be used.¹⁷ Even in the case of broad spectrum absorption materials, absorption of photons with energy higher than the donor bandgap leads to a thermalization loss. Phase

separation between the donor and acceptor materials should be within the exciton diffusion length for efficient exciton dissociation necessitating the donor–acceptor morphology at nanoscale dimensions.^{18,19} In addition, proper electrode selection should favor efficient charge collection. Based on careful consideration of these criteria, the recently reported power conversion efficiency (PCE) for single junction polymer solar cells is 11.1%. However, further efficiency increase in single junction solar cells will be limited by the thermalization loss and energy loss required for exciton dissociation.^{3,20,21} Multijunction polymer solar cells based on different polymers with different bandgaps for complementary spectrum absorption can be used to reduce these losses and achieve high efficiency. This requires the combination of both large and small bandgap polymers. Large bandgap (2 eV) polymers include poly(2-methoxy-5-(28-ethylhexyloxy)-*p*-phenylene-vinylene) (MEH-PPV),²² poly(2-methoxy-5-(3',7'-dimethyloctyl)-*p*-phenylenevinylene) (MDMO-PPV),²³ and



Olusegun Adebajo received a BSc degree in physics from Obafemi Awolowo University, Ile-Ife, Nigeria in 2004 and a MSc degree in optoelectronic and communications engineering from Northumbria University, Newcastle, UK in 2010. His MSc research focussed on the free-space optical communication system under the direction of Prof. Zabih Ghassemloo. He then joined

the Organic Electronics Laboratory of South Dakota State University, USA in 2012. Presently, he is pursuing his PhD under the supervision of Dr Qiquan Qiao in the area of polymer multi-junction solar cells.



Prajwal Adhikary received his Bachelor's degree in electronics and communication engineering from the Cosmos College of Management and Technology, Pokhara University, Kathmandu, Nepal. He is currently working on inverted polymer organic solar cells under the supervision of Dr Qiquan Qiao at South Dakota State University. His current research includes improvement of elec-

tronic properties of electron transport layers for application in inverted polymer organic solar cells.



Purna P. Maharjan received his Bachelor's degree in electrical engineering from the Institute of Engineering, Tribhuvan University, Kathmandu, Nepal. He is currently working on Organic Solar Cells (OSCs) under the supervision of Dr Qiquan Qiao at South Dakota State University. His research interest includes optimization of device fabrication processes for organic solar cells.



Dr Mingtai Wang received his PhD in polymer physics from the University of Science and Technology of China in 1997. After his postdoctoral research in nanomaterials at Institute of Solid State Physics (ISSP), Chinese Academy of Sciences (CAS), he joined the ISSP as an associate professor in 1999. He worked at Institute of Polymer Research Dresden, Germany as a visiting scientist and Alexander

von Humboldt research fellow during 2000–2003. He became a full professor of materials physics and chemistry in the Institute of Plasma Physics at Hefei Institute of Physical Sciences, CAS under the support of "100-talent Program" in 2004. He is leading a group that mainly studies the materials and device performance in polymer solar cells.

poly(3-hexyl-thiophene) (P3HT).²⁴ Among these, P3HT is the most commonly used donor in front subcells of multijunction structures.²⁵ Low bandgap polymers such as poly(diketopyrrolopyrrole-terthiophene) (PDPP3T)²⁶ and poly[(4,4'-bis(2-ethylhexyl)-dithieno[3,2-b:2',3'-d]silole)-2,6-diyl-*alt*-(2,1,3-benzothiadiazole)-4,7-diyl] (PSBTBT)²⁷ are frequently used as donors in back subcells of double junction devices. Fullerene and its derivatives such as (6,6)-phenyl-C61-butyric acid methyl ester (PC₆₀BM) and (6,6)-phenyl-C71-butyric acid methyl ester (PC₇₀BM) have been widely used as acceptors due to their suitable electron affinity and mobility.²⁸ Currently, double junction polymer solar cells show an efficiency of 10.6%.²⁹ Recently Li *et al.* from the Janssen group reported a triple junction polymer solar cell with an efficiency of 9.64% using poly[*N*-9'-hepta-decanyl-2,7-carbazole-*alt*-5,5-(4',7'-di-2-thienyl-2',1',3'-benzothiadiazole)] (PCDTBT) in the front cell, and poly[2,5-bis(2-hexyldecyl-2,3,5,6-tetrahydro-3,6-dioxopyrrolo[3,4c]pyrrole-1,4-diyl)-*alt*-[3',3'-dimethyl-2,2':5',2''-terthiophene]-5,5-diyl] (PMDPP3T) in the middle and back cells.³⁰ Tandem polymer solar cell development has also been recently reviewed by others.^{31,32}

In this article, developments in triple junction polymer solar cells are reviewed. First, the efficiency prediction for triple and quadruple junction polymer solar cells and their dependence on subcell bandgaps, cutoff absorption wavelengths and active layer thicknesses are discussed. Second, fullerene derivative based acceptors, wide and low bandgap donor polymers and intermediate layer materials are described. Third, recent performance evolution with efficiencies up to 9.64% in triple junction polymer solar cells is reviewed. Finally, future directions in triple junction devices are briefly discussed.

2. Efficiency prediction for series connected triple junction polymer solar cells

Fig. 1 shows the energy level alignment of a series connected triple junction polymer solar cell. In the series structure, light absorption with complementary spectral ranges generates excitons in each subcell. Electrons move from one subcell to the intermediate layer and recombine with the holes from the next subcell.³ The overall triple junction cell current is limited by the subcell with the lowest current density. One requirement in series connected multijunction cells is that the currents from each subcell should match. Individual subcell currents can be engineered to be equal by selecting appropriate light absorbers and varying the active layer thickness.

The series connected triple junction solar cell open circuit voltage (V_{oc}) can be as high as the sum of individual subcells V_{oc} as

$$V_{oc-multi} = V_{oc1} + V_{oc2} + V_{oc3} \quad (1)$$

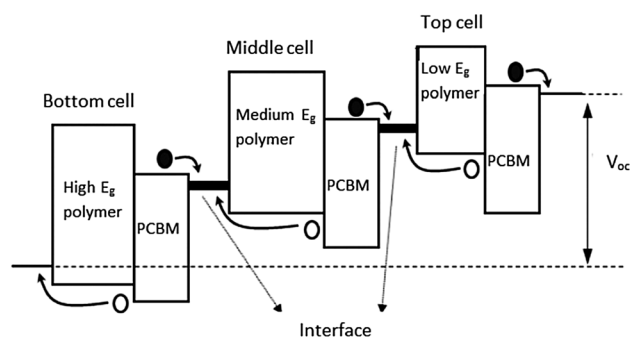
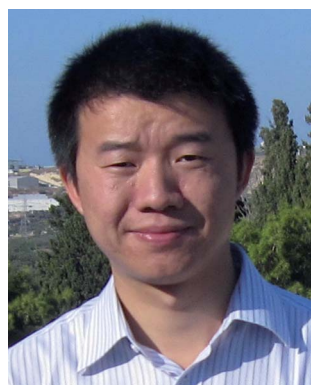


Fig. 1 Band diagram of a triple junction polymer solar cell in a series connection under the open circuit voltage condition. Reproduced with permission from ref. 3.



Dr Shangfeng Yang received his PhD from the Hong Kong University of Science and Technology in 2003. He then joined the Leibniz-Institute for Solid State and Materials Research (IFW) Dresden, Germany as an Alexander von Humboldt (AvH) Fellow (2004–2005) and a Guest Scientist (2005–2007). In Dec. 2007 he joined the University of Science and Technology of China as a professor at the Hefei

National Laboratory for Physical Sciences at Microscale & Department of Materials Science and Engineering, awarded by “Hundreds of Talents Programme” of Chinese Academy of Sciences. His current research interests include the synthesis of novel carbon nanostructures and their applications in organic solar cells.



Dr Qiquan Qiao is an associate professor of Electrical Engineering. After completing his postdoctoral research with Prof. John Reynolds at University of Florida, he joined as a faculty member in the Department of Electrical Engineering and Computer Sciences at South Dakota State University (SDSU), where he established the Organic Electronics Laboratory. His current research focuses on

polymer photovoltaics and dye-sensitized solar cell materials and devices. He received the 2009 Bergmann Memorial Award from the US-Israel Bi-national Science Foundation (BSF), 2010 US NSF CAREER Award, and 2012 College of Engineering Young Investigator Award. During his graduate study, Dr Qiao received the 2006 American Society of Mechanical Engineers Solar Energy Division Graduate Student Award and the 2006 Chinese Government Award for Outstanding Students Abroad.

where V_{oc1} , V_{oc2} , and V_{oc3} are the individual subcell open circuit voltages.

The maximum V_{oc} of individual subcells is estimated from the difference between the acceptor LUMO and the donor HOMO as:

$$V_{oc(i)} = \frac{1}{e} (\text{LUMO}_{\text{acceptor}(i)} - \text{HOMO}_{\text{donor}(i)}) \quad (2)$$

where e is the elementary charge, $\text{LUMO}_{\text{acceptor}(i)}$ and $\text{HOMO}_{\text{donor}(i)}$ are the acceptor LUMO and the donor HOMO in the i^{th} subcell, respectively. Empirically, this equation has been revised as:³³

$$V_{oc} = \frac{1}{e} (\text{LUMO}_{\text{PCBM}} - \text{HOMO}_{\text{polymer}} - 0.3 \text{ eV}) \quad (3)$$

where the empirical 0.3 eV was the deviation from the maximum open circuit voltage (V_{oc}) estimated from eqn (2). The individual subcell V_{oc} can be increased by moving the acceptor LUMO closer to the vacuum level and/or pushing the donor HOMO away from the vacuum level with a minimum offset required for efficient charge transfer from the donor to the acceptor.^{34,35} If there are no intermediate layers to function as recombination/tunnelling layers, a multiple junction cell in a series connection would result in an inversely oriented donor-acceptor (D-A) junction where one subcell is directly stacked on the other. Then carriers will build up in the reverse D-A junction and reduce the overall device V_{oc} .³⁶ This requires that interfacial recombination/tunnelling layers must be used between the adjacent individual subcells.

In a multijunction device, the first subcell short circuit current density (J_{sc1}) is given by

$$J_{sc1} = \int_{\lambda_0}^{\lambda_1} e N_{ph}(\lambda) EQE_1(\lambda) d\lambda \quad (4)$$

Here, $EQE_1(\lambda)$ and $N_{ph}(\lambda)$ are the external quantum efficiency and photon flux density, respectively. λ_0 and λ_1 define the first subcell absorption spectrum range.

The J_{sci} of the i^{th} subcell in a multijunction device can be simplified as

$$J_{sc-i} = \int_{\lambda_{i-1}}^{\lambda_i} e N_{ph}(\lambda) EQE_i(\lambda) d\lambda \quad (5)$$

where λ_{i-1} and λ_i define the i^{th} subcell absorption spectrum range. For simplicity, we assumed that the prior subcells absorb all the photons with energy higher than λ_{i-1} . Therefore the i^{th} subcell is assumed to only harvest the photons between λ_{i-1} and λ_i . The multijunction cell efficiency in a series connection is estimated by

$$\eta_{\text{multi}} = \frac{J_{sc\text{-multi}} V_{oc\text{-multi}} FF}{P_{\text{light}}} \quad (6)$$

where the FF can be enhanced by engineering film morphology and various interfaces in both individual subcells and between subcells.^{37,38}

2.1. Dependence of efficiency on subcell bandgaps

We have performed calculation on multijunction polymer solar cells to identify the bandgaps in different subcells that are

needed for highly efficient multijunction polymer solar cells. The double junction device efficiency was calculated by continuously increasing the subcell bandgaps across the solar spectrum. The triple junction cell efficiency was obtained by fixing the front subcell bandgap at 1.9 eV and then continuously increasing the middle and top subcell bandgaps. Similarly in quadruple junction cells, the front and first middle subcell bandgaps were kept at 2.0 and 1.5 eV respectively, and the second middle and top cell bandgaps were continuously increased across the solar spectrum to calculate the overall device efficiency. Fig. 2 shows the calculated current density (J_{sc}) and efficiency (η) of 2J, 3J and 4J multijunction solar cells. The calculation was performed under the following presumptions: (1) subcells are series-connected with larger bandgap polymers used in the front. (2) Subcells absorb photons within their absorption spectral range. For example, in a 4J solar cell, the absorption cutoff wavelengths are λ_1 , λ_2 , λ_3 , and λ_4 in cell 1 through 4, respectively. The front subcell (cell 1) absorbs photons below λ_1 , the first middle subcell (cell 2) absorbs photons between λ_1 and λ_2 , the second middle subcell (cell 3) absorbs photons between λ_2 and λ_3 , and the back subcell (cell 4) absorbs light between λ_3 and λ_4 . (3) EQE is 65% and FF is 0.6. (4) V_{oc} of the individual subcells was calculated by subtracting E_g from the exciton binding energy (E_b), which was assumed as 0.3 eV. (6) The overall J_{sc} of multijunction solar cells is limited by the smallest J_{sc} among all the subcells. The overall multijunction device efficiency was obtained using eqn (6).

The above calculation was based on the ideal condition where we tried to match subcell J_{sc} and used the lowest subcell J_{sc} as the overall double and triple junction cell J_{sc} . However, some possible variations from the ideal condition also need to be discussed. Hadipour *et al.*³⁹ proposed a methodology for forecasting experimental tandem PCE by exaggerating component subcell device performance parameters. They considered two cases of a double junction tandem cell: (1) one subcell has a lower J_{sc} and sufficiently high FF connected serially to another subcell with higher J_{sc} and extremely low FF; (2) one subcell has a serial connection of higher J_{sc} and FF to another subcell with lower J_{sc} and FF. The former tandem cell results in a J_{sc} close to the lower subcell J_{sc} but the latter tandem device gives a J_{sc} close to the higher subcell J_{sc} . This has been supported by some reported work on tandem cell current density-voltage curves.⁴⁰⁻⁴³ The FF of tandem cells can also be higher than that of individual subcells from the literature⁴⁴⁻⁴⁶ The subcell active layer thickness can also be used to optimize the J_{sc} in the tandem and multijunction devices. Boland *et al.*,⁴⁷ Nam *et al.*⁴⁸ and Namkoong *et al.*⁴⁹ reported new models by combining the optical and drift diffusion models in order to simulate and understand the optical field distribution in tandem with the charge transport phenomenon. Their simulated results provided consistency with experimental data, but they based their study on identical conjugated polymer:acceptor pairs in the front and back subcells; hence extension of this model to other materials in tandem devices is necessary. This implies that estimation of device performance parameters is not that straightforward as it still requires further investigation to fully understand and predict the tandem performance from

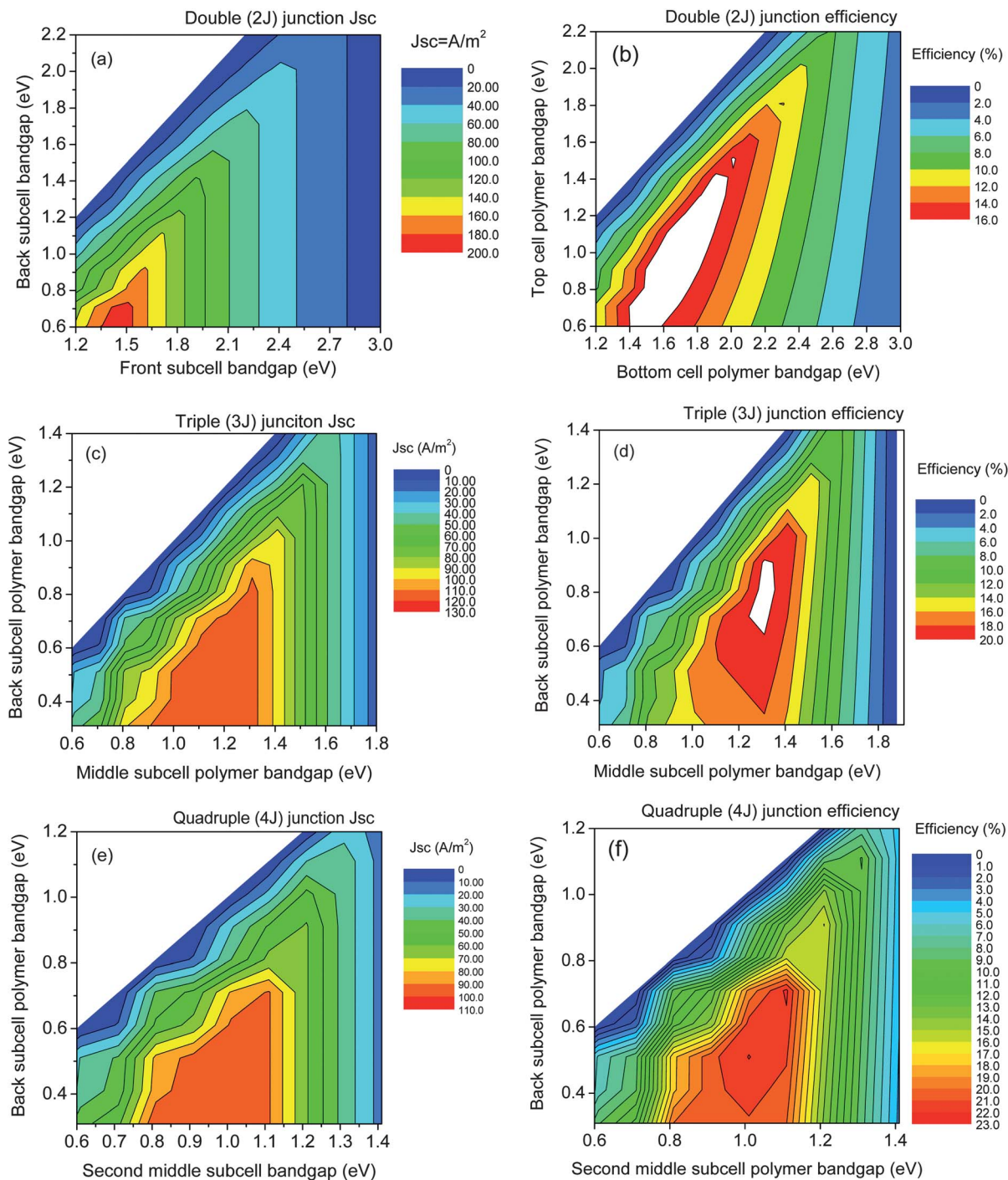


Fig. 2 Dependence of the current density (J_{sc}) of (a) double, (c) triple and (e) quadruple junctions, and efficiency (η) of (b) double, (d) triple and (f) quadruple junction solar cells on the subcell bandgap.

component subcells, over a broad range of material selections and processing methods, with relatively high accuracy. Such an understanding will give a device designer the leeway to optimize a dominating performance parameter for obtaining higher efficiency in tandem PSCs.

As shown in Fig. 2a, the decrease of bandgaps in the front and back subcells can increase the overall J_{sc} of double junction (2J) solar cells. The red region located at the center point of

(~ 1.5 eV for the front subcell, ~ 0.6 eV for the back subcell) shows a J_{sc} of up to 200 A m^{-2} . However, a smaller bandgap can also reduce V_{oc} , which is another important parameter for obtaining high efficiency. A balance between J_{sc} and V_{oc} needs to be achieved for high device efficiency. Fig. 2b shows the dependence of double junction solar cell efficiency on subcell bandgaps. The white region with a center point at ~ 1.6 eV and ~ 1.0 eV shows an efficiency higher than 15%. This indicates

that the front and back subcell bandgaps within this white region can be selected to achieve the possible double junction cell efficiency higher than 15%. Fig. 2c and d show the dependence of current density and efficiency on middle and back subcell bandgaps for a triple junction (3J) cell. The red region located at the center point of ~ 1.2 eV and ~ 0.5 eV in Fig. 2c shows a J_{sc} of up to 130 A m^{-2} . The J_{sc} in the triple junction is smaller than that in the double junction because one more subcell shares the photons from the overall solar spectrum. To achieve an efficiency higher than 20% in triple junction polymer solar cells (Fig. 2d), the bandgaps of the middle and back subcells can be selected within the white region at the center point (~ 1.3 eV, ~ 0.9 eV). Fig. 2e and f represent the dependence of the current density and efficiency on second middle and back subcell bandgaps for a quadruple junction (4J) cell. The second middle and back subcell bandgaps can be placed in the red region with a center point at ~ 1.0 eV, and ~ 0.45 eV to achieve a J_{sc} of up to 110 A m^{-2} . As discussed above, this value is smaller than those of double and triple junction solar cells since more subcells are used to share the overall solar spectrum photons. For quadruple junction cells (Fig. 2f), the bandgaps of second middle and top subcells can be selected in the red region with a center point at ~ 1.05 eV and ~ 0.6 eV.

Fig. 3a shows the predicted dependence of the triple junction cell efficiency (η_{triple}), open circuit voltage ($V_{oc\text{-triple}}$), and short circuit current density ($J_{sc\text{-triple}}$) on the absorption spectrum of

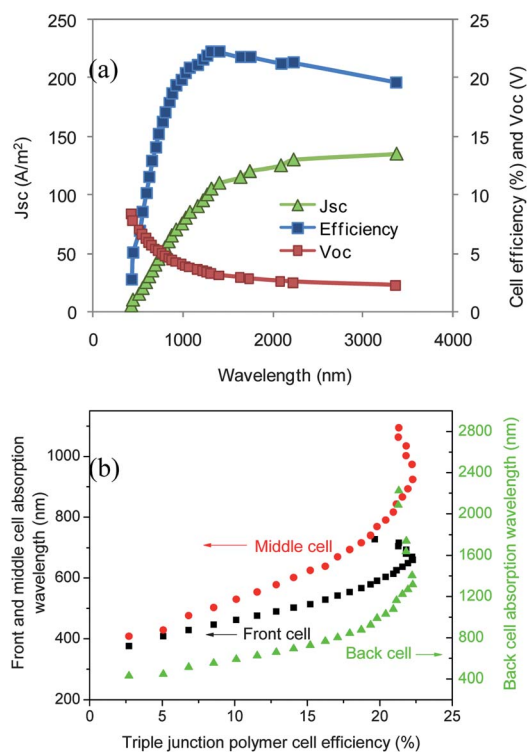


Fig. 3 (a) Calculated dependence of the triple junction cell efficiency (η_{triple}), open circuit voltage ($V_{oc\text{-triple}}$), and short circuit current density ($J_{sc\text{-triple}}$) on the entire cell absorption spectrum cutoff wavelength (reproduced with permission from ref. 3); and (b) relationship between the cell efficiency and the combination of subcell absorption spectrum cutoff wavelengths in the triple junction structure.

the entire device, in which each subcell was assumed to absorb the same amount of photons and generate matched current density.³ As shown in Fig. 3a, the triple junction cell $V_{oc\text{-triple}}$ decreases, while $J_{sc\text{-triple}}$ increases as the overall absorption spectrum broadens into longer wavelengths.³ With an assumption of FF = 0.6 and EQE = 65%, an efficiency of up to 22.3% is achievable.

Fig. 3b shows a combination of absorption spectrum cutoff wavelengths in all subcells in the triple junction structure. To achieve the highest possible device efficiency, the cutoff wavelengths of the front, middle and back cells should be ~ 660 nm (1.9 eV), ~ 924 nm (1.3 eV) and ~ 1350 nm (0.9 eV), respectively, which is consistent with the earlier discussion in Fig. 2d.

Fig. 3b also provides the combination of cutoff wavelengths from subcells in triple junction polymer solar cells to obtain efficiencies lower than 22.3%. It is interesting to find that the same device efficiency can be obtained from different combinations of subcell absorption spectra. For example, two different absorption combinations such as ~ 590 nm, ~ 770 nm, and ~ 990 nm or ~ 730 nm, ~ 1160 nm, and ~ 3365 nm for the respective front, middle and back subcells can be used to obtain the same cell efficiency at $\sim 19.7\%$ with FF = 0.6 and EQE = 65%. The reason that our calculated cell efficiency is lower than what Minnaert *et al.* have reported is that we used a lower EQE and FF, and a larger D–A LUMO offset.⁵⁰

2.2. Subcell active layer thickness effects on light absorption and cell performance

Double junction solar cells. In 2007, Dennler *et al.* performed optical simulations on tandem cells based on four photoactive blends incorporating P3HT and PCPDTBT polymers in blends of both PC₇₀BM and PC₆₀BM.⁵¹ They also studied the thickness effects on light absorption. Their results were then validated with experimental results earlier reported by Kim *et al.*⁵²

Fig. 4 shows the real and imaginary parts of the complex refractive indices of the four photoactive blends investigated.

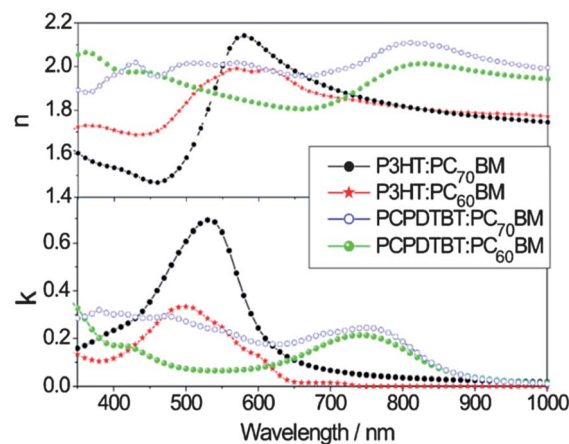


Fig. 4 Optical parameters (real and imaginary parts of the complex refractive indices) of various photoactive layers used in the simulations. Reproduced with permission from ref. 51.

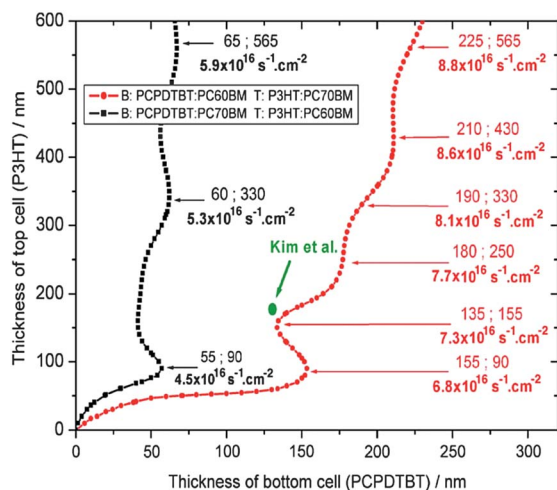


Fig. 5 Thickness of the P3HT based top cell vs. thickness of the PCPDTBT based bottom cell of two different donor–acceptor combinations in a tandem cell. The various points indicate the number of photons absorbed in both photoactive layers of the tandem while the green point represents the tandem work of Kim *et al.* Reproduced with permission from ref. 51.

Within the 350–700 nm wavelength range, the use of PC₇₀BM against PC₆₀BM enhanced the imaginary part of the complex refractive index (*i.e.* the extinction coefficient of the BHJ layer).

This increased visible-light absorption due to the asymmetry of PC₇₀BM molecules cause the lowest-energy transition possible compared to highly symmetric PC₆₀BM molecules which forbid such a transition.⁵³ As can be observed in Fig. 4, the minimum absorption of the PCPDTBT:PC₆₀BM blend coincided exactly with the maximum absorption of the P3HT:PC₇₀BM blend at around 500 nm, suggesting a nearly ideal active BHJ layer for tandem configuration. This coincidence explained the rationale behind the material selection employed by Kim *et al.*⁵² Dennler *et al.* further showed that a compromise must be reached between acceptor selection and thickness variation.⁵¹ Fig. 5 shows that a 65 nm thick PCPDTBT:PC₇₀BM blend as the bottom cell will require a ~565 nm thick P3HT:PC₆₀BM blend as the top cell in order to absorb a photon flux of $5.9 \times 10^{16} s^{-1} cm^{-2}$. However, a bottom cell with 135 nm thick PCPDTBT:PC₆₀BM will only require a top cell with 155 nm thick P3HT:PC₇₀BM blend for harvesting a higher photon flux of $7.3 \times 10^{16} s^{-1} cm^{-2}$. It is important to note that low bandgap PCPDTBT and wide bandgap P3HT were used as bottom and top subcells respectively to maximize photon absorption. This analyzed result was consistent with the experimental work by Kim *et al.* in which PCPDTBT:PC₆₀BM and P3HT:PC₇₀BM blends were ~130 nm and ~200 nm thick, respectively.⁵²

Fig. 6 shows the dependence of calculated double junction solar cell parameters on the thickness of the front and back

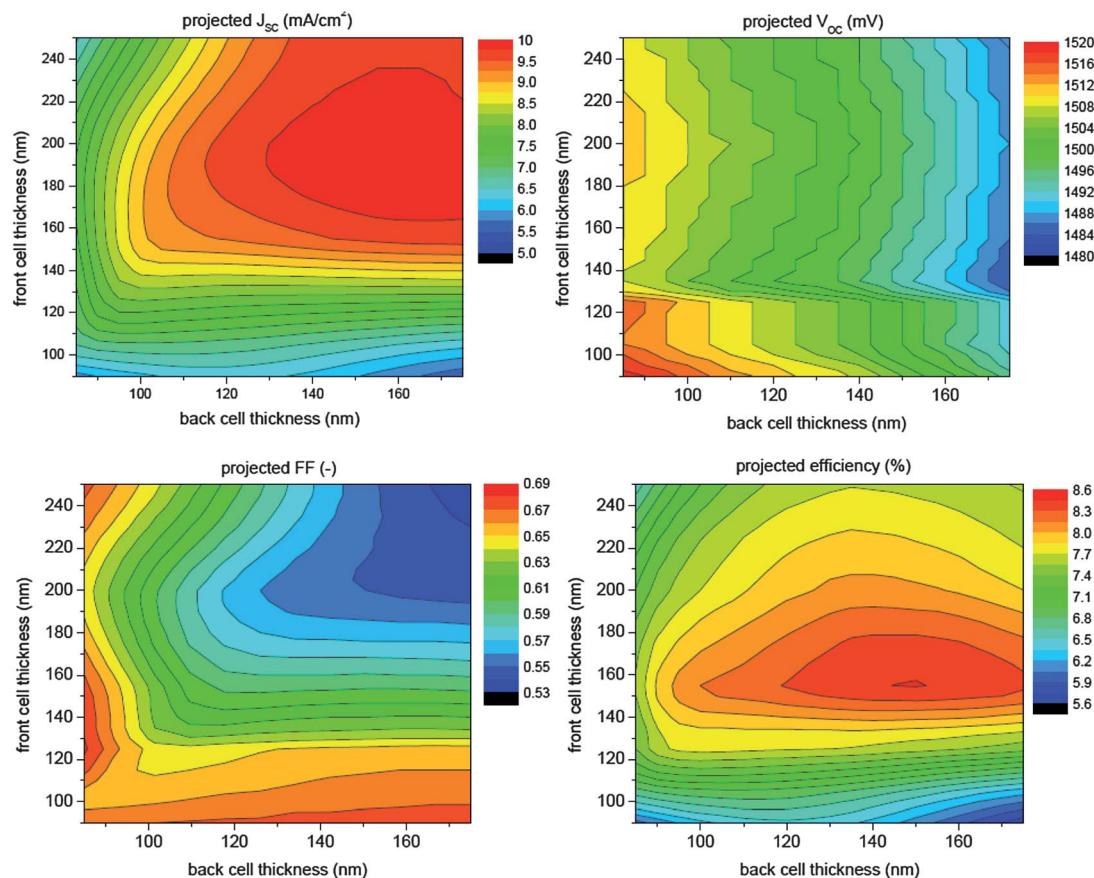


Fig. 6 Dependence of calculated solar cell parameters on the thicknesses of front and back cells in the double junction structure. The front cell is PCPDTBT:PC₇₀BM and the back cell is PMDPP3T:PC₆₀BM. Reproduced with permission from ref. 30.

cells, reported by Li *et al.* from the Janssen group in 2013.³⁰ The front cell is PCDTBT:PC₇₀BM and the back cell is PMDPP3T:PC₆₀BM. A high short circuit current density (J_{sc}) requires a back cell active layer thickness >110 nm and a front cell thickness >140 nm, as shown in the top right red region in Fig. 6a. However, a high open circuit voltage (V_{oc}) needs a lower thickness in both the front and back subcell active layers (see the bottom left red region in Fig. 6b). In addition, a high fill factor (FF) requires a lower thickness in either the front or back subcell active layers (left red or bottom red region in Fig. 6c). By combining the effects of J_{sc} , V_{oc} and FF in the double junction solar cells, the thicknesses need to be ~140–180 nm for the front cell and ~130–170 nm for the back cell to obtain an efficiency larger than 8%. The highest efficiency of 8.5% is expected with a front active layer thickness of 155 nm and a back cell thickness of 150 nm.³⁰ Using the optimized subcell thicknesses, the authors have experimentally achieved double junction solar cell efficiencies above 8.4% with the highest value of 8.9%.³⁰ Earlier in 2010, a similar study on thickness variation was demonstrated by Gilot *et al.* from the same research group to predict the performance of a tandem device by combining optical absorption analysis with electrical characteristics of individual single-junction subcells of the tandem device.⁴²

Triple junction solar cells. Li *et al.* also predicted the relationship between the triple junction polymer solar cell efficiency and the subcell thicknesses (Fig. 7).³⁰ The authors determined the optimal subcell thicknesses to be 125 nm, 95 nm, and 215 nm for front, middle and back cells, respectively. They fabricated triple junction devices and achieved an average efficiency of 9.3% with the highest efficiency at 9.6%. It is important to mention that the aim of this reported work is to split the small bandgap polymer (PMDPP3T:PC₆₀BM) layer into two junctions to provide a surplus of photocurrent due to the limitation in photocurrent generation in the wide bandgap polymer (PCDTBT:PC₇₀BM) layer. This methodology is different

from that of using a triple junction cell which is to broaden the absorption to as long a wavelength as possible.

3. Advances in acceptor, donor and interconnecting layer materials

New material development through chemical structure engineering of fullerene derivatives and wide and low bandgap polymers has played a critical role in increasing the organic solar cell efficiency to 11.1%, 10.6%²⁹ and 9.64%³⁰ for single, double and triple junction devices, respectively. Although numerous materials have been reported in the literature, emphasis here will be made on those materials that have led to efficient multijunction devices in recent years. In order to reduce the thermalization losses, wide bandgap polymers are typically used in multijunction organic solar cells to absorb large energy photons in the front subcells and low bandgap polymers are used to absorb low energy photons in back subcells.

3.1. Acceptor materials

In 1992, Sariciftci *et al.* observed a sub-picosecond electron transfer from the excited state of the conjugated polymer to C₆₀,^{56,57} which formed the basis of polymer:fullerene solar cells. C₆₀ derivatives such as PC₆₀BM and PC₇₀BM are more soluble than C₆₀ and C₇₀, leading to the concept of bulk heterojunction structure from the earlier adopted bilayer architecture.⁵⁸ This newer concept solved the low exciton diffusion length issue and significantly improved the device performance. Both [60]PCBM and [70]PCBM are efficient electron acceptors with high electron mobility. However, PC₇₀BM was frequently found to have higher efficiency than PC₆₀BM due to its higher lying LUMO and additional light absorption in the 400–700 nm region of the solar spectrum.⁵⁹ Researchers have modified the fullerene derivatives' chemical structures to raise the acceptor LUMO for higher V_{oc} in polymer solar cells. For example, the indene-C₆₀-bisadduct (IC₆₀BA) and indene-C₇₀-bisadduct (IC₇₀BA) have been used in the literature to increase V_{oc} from 0.6 V to 0.8 V and PCE from ~5% to 5.5–6.5% in single junction cells when PC₆₀BM/PC₇₀BM was changed to IC₆₀BA/IC₇₀BA.^{55,60} By using ICBA, double junction solar cells have achieved an efficiency of 8.6%,⁴¹ which was recently increased to 10.6%.²⁹ In addition, other fullerene derivatives,^{61–63} *n*-type polymeric⁶⁴ and molecular acceptors⁶⁵ have been synthesized and used as acceptors in polymer solar cells but with a lower efficiency than ICBA. Table 1 shows a non-exhaustive list of fullerene derivatives that have been employed in multijunction polymer solar cells. Key fullerene derivative parameters including the chemical structure, HOMO, LUMO, and bandgap are also included in Table 1.

3.2. Wide bandgap conjugated donor materials

Fig. 8 shows typical wide bandgap polymers that have been integrated into the double junction polymer solar cell architecture. The first group of wide bandgap ($E_g = \sim 1.9\text{--}2.3$ eV) donor materials are poly(phenylenevinylene) (PPV) based

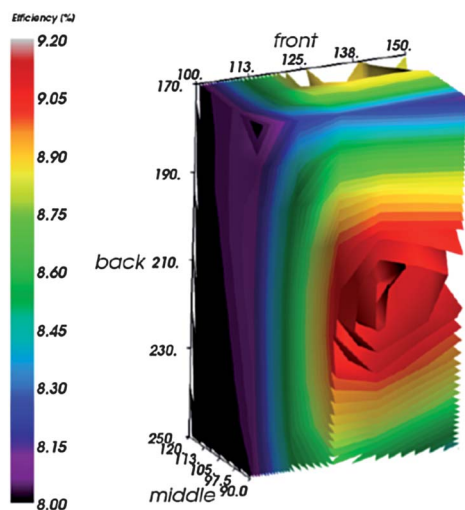
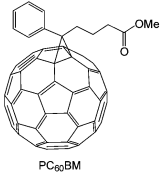
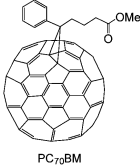
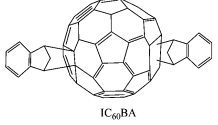
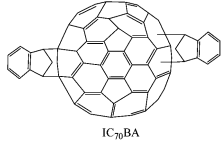
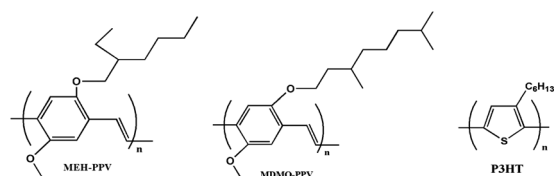
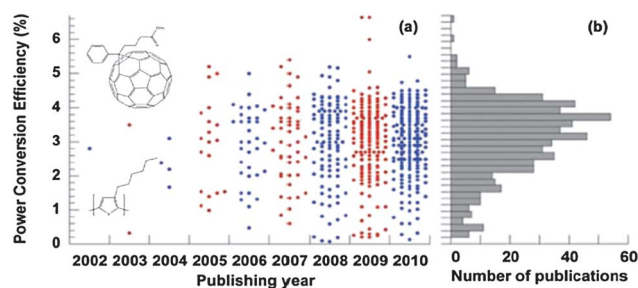


Fig. 7 Calculated triple junction solar cell efficiency dependence on the subcell thickness. Front subcell: PCDTBT:PC₇₀BM, middle and back subcell: PMDPP3T:PC₆₀BM and back. Reproduced with permission from ref. 30.

Table 1 Non-exhaustive list of typical acceptor materials

Structure	Name	HOMO (eV)	LUMO (eV)	Band-gap (eV)	Ref.
	[60]PCBM: [6,6]-phenyl C ₆₁ butyric acid methyl ester	-6.1	-4.3	1.8	52
	[70]PCBM: [6,6]-phenyl C ₇₁ butyric acid methyl ester	-6.1	-3.7	2.4	54
	indene-C ₆₀ -bisadduct	-5.8	-3.7	2.1	41
	indene-C ₇₀ -bisadduct	-5.61	-3.72	1.89	55

polymers including poly(2-methoxy,5-(2'-ethyl-hexyloxy)-*p*-phenylenevinylene) (MEH-PPV) and poly(2-methoxy-5-(3',7'-dimethyloctyl)-*p*-phenylenevinylene) (MDMO-PPV). Such PPV-based polymers have poor light absorption in red and near infrared regions and low hole mobility, leading to a low efficiency of ~3%.⁵³ Another group of wide bandgap polymers are polythiophenes and their derivatives. For example, regioregular poly(3-hexyl-thiophene) (rr-P3HT) is the most widely used due to its preferential interchain packing and higher hole mobility reducing the propensity for the current limitation from the space charge effect.^{14,66} Fig. 9 shows the number of publications reporting the use of P3HT in single, double and multijunction polymer solar cells surveyed between 2002 and 2010. It has been shown that higher hole mobility can be achieved through control of active layer growth by methods such as solvent annealing which provides ordered rearrangement of the components and reduces defects at the metal-semiconductor interface⁶⁷ and thermal annealing which allows the

**Fig. 8** Chemical structures of typical wide bandgap donor materials employed in double and multi-junction polymer solar cells.**Fig. 9** (a) Reported power conversion efficiencies (PCEs) of solar cells incorporating the P3HT:PCBM active layer surveyed in 579 publications with each dot representing the reported maximum PCE value in each publication and the inset depicting P3HT and PCBM chemical structures. (b) Overall PCE value distribution from 2002 to 2010. Reprinted with permission from ref. 25.

reorganization and crystallization of the component phases.^{13,68,69} In addition, P3HT exhibits the favorable 1 : 1 weight ratio with fullerene allowing optimal use of conjugated polymers unlike other polymers such as PPVs with 1 : 2, 1 : 3 or 1 : 4 weight ratios. PCEs of 4–5% have been reported for P3HT:fullerene based devices.^{25,70} In addition, P3HT also dominates as wide bandgap polymers for use in double and multijunction solar cells. Researchers have also tried to engineer the chemical structure of polythiophene-based polymers to increase V_{oc} by lowering HOMO of conjugated polymers. Hu *et al.*⁷¹ synthesized an ester group functionalized derivative of polythiophene. Hou *et al.*⁷² reduced the number of alkyl side-chains to decrease the electron donating effect of alkyl side-chains. Ko *et al.*⁷³ introduced a '3,4-dialkyl' side-chain into polythiophene. The V_{oc} enhancement was significant.

3.3. Low bandgap conjugated polymers

In 2001, the Janssen group first reported a low bandgap copolymerization of electron-deficient 2,1,3-benzothiadiazole (BT) and electron rich thiophene that enabled longer wavelength photon absorption up to 900 nm. They used it in polymer-fullerene solar cells with a PCE less than 0.5%.⁷⁴ Then in 2006, PCPDTBT based on BT and the 4*H*-cyclopenta[2,1-*b*:3,4-*b'*]-dithiophene (CPDT) alternating copolymer was used in single junction solar cells and a PCE of 3.5% was achieved due to its high hole mobility, extended conjugation and strong intermolecular interaction.⁷⁵ Later on, an efficiency higher than 5% was obtained after a small amount of octane 1,8-dithiol was added as an additive to the processing solvent.⁷⁶ In 2007, Blouin *et al.* synthesized poly[*N*-9'-hepta-decanyl-2,7-carbazole-*alt*-5,5-(4',7'-di-2-thienyl-2',1',3'-benzothiadiazole)](PCDTBT) that exhibited an initial efficiency of 3.6%,⁷⁷ which was later increased to 6.1% by introducing a TiO_x optical spacer.³⁵ In 2008, Hou *et al.* designed and synthesized poly[(4,4'-bis(2-ethylhexyl)dithieno[3,2-*b*:2',3-*d*]silole)-2,6-diyl-*alt*-(2,1,3-benzo-thiadiazole)-4,7-diyl](PSBTBT),²⁷ which also exhibited an efficiency higher than 5%. In 2010, Bijleveld *et al.* synthesized (poly[{2,5-bis(2-hexyldecyl)-2,3,5,6-tetrahydro-3,6-dioxopyrrolo[3,4-]pyrrole-1,4-diyl}-*alt*-{2,2'-(1,4-phenylene)bisthiophene}-5,5'-diyl}]) (PDPPTPT) which is based on the diketopyrrolo-pyrrole (DPP) unit copolymerized with thiophene and a blend of PC₆₀BM and PC₇₀BM, which

showed 4.6% and 5.5% efficiencies respectively.⁷⁸ Subsequently in 2011, Bronstein *et al.* replaced the thiophene with larger thieno[3,2-*b*]thiophene units and achieved an efficiency of 5.4% with PC₇₀BM.⁷⁹

In 2008, Liang *et al.* synthesized a new polymer (PTB1) through the design and preparation of alternating units of thieno[3,4-*b*]thiophene (TT) and benzodithiophene (BDT). The repeat unit of TT was known to stabilize the quinoidal structure of the backbone which narrowed the resulting polymer bandgap while the ester substitution ensured the solubility and oxidative stability. Single junction polymer solar cells using PTB1 as the donor and PC₆₀BM and PC₇₀BM as acceptors resulted in efficiencies of 4.76% and 5.3% respectively.⁸⁰ Similarly, Chen *et al.* in 2009 used different functional groups on poly[4,8-bis-substituted-benzo[1,2-*b*:4,5-*b'*]dithiophene-2,6-diyl-*alt*-4-substituted-thieno[3,4-*b*]thiophene-2,6-diyl (PBDTTT) to enhance the V_{oc} and efficiency. Three synthesized conjugated polymers including PBDTTT-E, PBDTTT-C and PBDTTT-CF exhibited a V_{oc} of 0.62 V, 0.70 V and 0.76 V and an efficiency of 5.15%, 6.58% and 7.73% respectively.³⁴

In 2010, Bijleveld *et al.* synthesized (poly[{2,5-bis(2-hexyldecyl)-2,3,5,6-tetrahydro-3,6-dioxopyrrolo[3,4-*b*]pyrrole-1,4-diyl-*alt*-{[2,2'-(1,4-phenylene)bisthiophene]-5,5'-diyl}}] (PDPPTPT) by copolymerizing the diketo-pyrrolo-pyrrole (DPP) unit with electron rich thiophene. A phenyl ring was also incorporated between adjacent thiophene rings. When PDPPTPT was blended with PC₆₀BM and PC₇₀BM to fabricate devices, they achieved an efficiency of 4.6% and 5.5% respectively.⁷⁸ Subsequently in 2011, Bronstein *et al.* replaced the thiophene with larger thieno[3,2-*b*]thiophene units and achieved an efficiency of 5.4% with PC₇₀BM.⁷⁹ In 2012, Dou *et al.* copolymerized BDT and DPP units to prepare a low bandgap polymer, poly{2,6'-4,8-di(5-ethylhexylthienyl)benzo[1,2-*b*;3,4-*b*]dithiophene-*alt*-5-dibutylloctyl-3,6-bis(5-bromothiophen-2-yl)pyrrolo[3,4-*c*]pyrrole-1,4-dione} (PBDTT-DPP), which exhibited good solubility, high molecular weight and high carrier mobility. This polymer resulted in 6.5% efficiency in single junction regular and inverted structures.⁴¹ Later in 2012, Dou *et al.* introduced different functional groups into BDT and DPP units resulting in cell efficiencies of 5.8–6.6%.⁸¹ Most of the above low bandgap polymers have been successfully incorporated as subcell active layers in high efficiency double junction polymer solar cells to be discussed in the later section. Table 2 shows a non-exhaustive list of the molecular structures of various low bandgap polymers that have been employed in double and triple junction polymer solar cells. Key polymer parameters including the chemical structure, HOMO, LUMO, bandgap, and the experimentally achieved efficiencies in single and multijunction devices are also included in Table 2.

One of the requirements for stacking two or more subcells to form multijunction solar cells is that the donor polymer in each subcell should have complementary absorption spectra. Fig. 10 shows an absorbance measurement illustrating the optical absorption densities and absorption band of several representative wide bandgap (P3HT and MDMO-PPV) and low bandgap (PSBTBT and PDPP3T) polymers blended with fullerene derivatives.

Critical challenges related to triple and quadruple junction devices are that existing polymers still do not meet the requirement of having all bandgaps and complementary absorption spectra from different polymers identified as shown in Fig. 2 and 3. Therefore, synthesis of low bandgap polymers to meet triple and quadruple junction device requirements is still an outstanding opportunity. Donor polymers particularly with bandgaps of ~ 0.9 eV for the third (top) junction in triple junction devices are still lacking experimental demonstration. To develop an efficient triple junction polymer solar cell with complementary absorption spectra, the polymers with required bandgaps for front and middle subcells have been demonstrated with high efficiency in double junction devices. Also the interconnecting layers that have been demonstrated in double junction cells can be used in triple junction devices.³⁰ Therefore, one of the real current challenges to fabricate high efficiency triple junction devices with complementary absorption spectra is the lack of polymers with the required bandgaps (~ 0.9 eV) for the third (top) subcells.

This polymer should also have an appropriate LUMO compared to that of acceptors at their interface leading to an offset not less than 0.3 eV for efficient exciton dissociation. In addition, the polymer HOMO should be low-lying in order to achieve high V_{oc} in subcells. Simultaneous engineering of the electronic and optical properties of polymers to achieve these two conditions requires conscientious efforts. Most of the recent designs and syntheses of conjugated polymers have been aimed towards lowering their HOMO energy levels as can be observed in Table 2. One widely adopted strategy employed to achieve this is the use of a number of 'push' and 'pull' units. By combining electron-rich units (*e.g.* thiophene-incorporated) and electron-deficient units (*e.g.* BT- or DPP-incorporated) in the polymer backbone in a 'push-pull' copolymer configuration, the HOMO and LUMO energy levels can be independently engineered.^{75,79} Another strategy is the stabilization of the quinoidal structure (*e.g.* from the TT unit) resulting in a low bandgap polymer followed by introduction of fluorine into TT to further achieve low-lying HOMO.⁸⁵ The rationale for this research direction is to enhance V_{oc} ⁸⁶ and improve the air-stability⁸⁷ of conjugated polymers. Development of low bandgap polymers with low-lying HOMO energy levels is the current research direction, and for achieving efficient triple junction cells, the third junction should have a bandgap of ~ 0.9 eV from our simulation result. Then the LUMO energy level of such polymers should be at least 0.3 eV, higher than the LUMO of acceptors. One possible alternative approach is to develop novel fullerene derivatives or chemically modify them as acceptors with tunable energy levels (LUMOs and HOMOs) specifically for low bandgap polymers that will not need strict requirements for the polymer LUMOs and HOMOs. This area of research has not been fully explored. In addition to the required bandgap and energy levels such as LUMOs and HOMOs, the polymers also need to have good solubility, high hole mobility and controllable morphology when blended with acceptors such as fullerene derivatives. All these need to be considered when designing new polymers and it is a critical need for transformative research in synthesizing novel low bandgap polymers

Table 2 Non-exhaustive list of typical low bandgap polymer donor materials in PMSCs

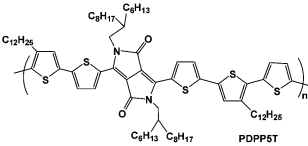
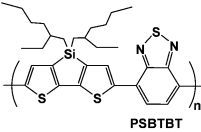
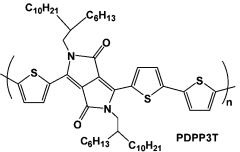
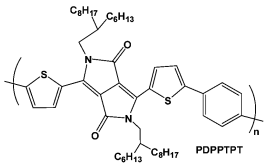
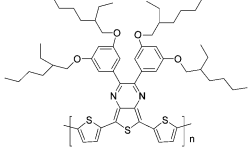
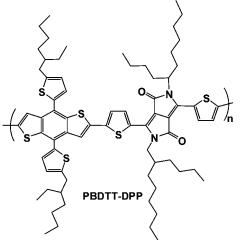
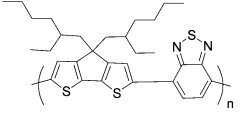
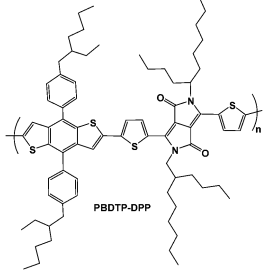
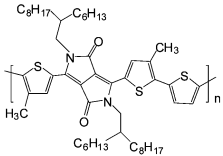
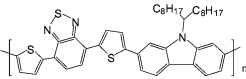
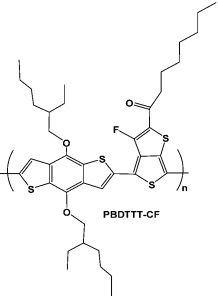
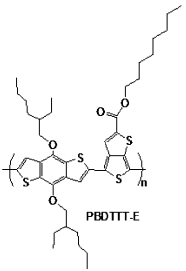
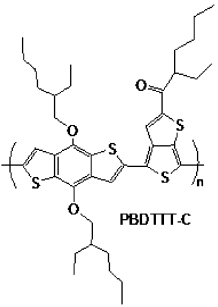
Structure	Name	HOMO (eV)	LUMO (eV)	Bandgap (eV)	Cell efficiency (%)		Ref.
					Single-junction	Multi-junction	
	PDPP5T: poly(diketopyrrolopyrrole-quintetthiophene)	-5.12	-3.55	1.32	5.3	7.0	82 and 45
	PSBTBT: dithieno[3,2- <i>b</i> :2',3'- <i>d</i>]silole polymer, poly[(4,4'-bis(2-ethylhexyl)dithieno[3,2- <i>b</i> :2',3'- <i>d</i>]silole)-2,6-diyl- <i>alt</i> -(2,1,3-benzothiadiazole)-4,7-diyl]	-5.05	-3.27	1.45	4.7	7.0	27 and 40
	PDPP3T: poly(diketopyrrolopyrrole-terthiophene)	-5.17	-3.61	1.30	4.7	—	26
	PDPPTPT: (poly[{2,5-bis(2-hexyldecyl)-2,3,5,6-tetrahydro-3,6-dioxopyrrolo[3,4- <i>c</i>]pyrrole-1,4-diyl}- <i>alt</i> -{[2,2'-(1,4-phenylene)bisthiophene]-5,5'-diyl}]	-5.35	-3.53	1.53	5.5	—	78
	PTBEHT: poly(5,7-di-2-thienyl-2,3-bis(3,5-di(2-ethylhexyloxy)phenyl)thieno[3,4- <i>b</i>]pyrazine	—	—	1.2	1.1	0.57	83
	PBDTT-DPP: poly{2,6'-4,8-di(5-ethylhexylthienyl)benzo[1,2- <i>b</i> ; 3,4- <i>b'</i>]dithiophene- <i>alt</i> -5-dibutyloctyl-3,6-bis(5-bromothiophen-2-yl)pyrrolo[3,4- <i>c</i>]pyrrole-1,4-dione}	-5.30	-3.63	1.44	6.5	8.62	41
	PCPDTBT: poly[2,6-(4,4-bis(2-ethylhexyl)-4 <i>H</i> -cyclopenta[2,1- <i>b</i> ; 3,4- <i>b'</i>]dithiophene- <i>alt</i> -4,7-(2,1,3-benzothiadiazole)]	-4.9	-3.5	1.4	3.2%	6.5%	52 and 75
	PBDTP-DPP: poly{2,6'-4,8-di(5-ethylhexylthienyl)benzo[1,2- <i>b</i> ; 3,4- <i>b'</i>]dithiophene- <i>alt</i> -5-dibutyloctyl-3,6-bis(5-bromothiophen-2-yl)pyrrolo[3,4- <i>c</i>]pyrrole-1,4-dione}	-5.35	-3.56	1.46	6.2	8.5	81

Table 2 (Contd.)

Structure	Name	HOMO (eV)	LUMO (eV)	Bandgap (eV)	Cell efficiency (%)		Ref.
					Single-junction	Multi-junction	
	PMDPP3T: poly[[2,5-bis(2-hexyldecyl-2,3,5,6-tetrahydro-3,6-dioxopyrrolo[3,4' <i>c</i>]pyrrole-1,4-diyl)- <i>alt</i> -[3',3''-dimethyl-2,2':5',2''-terthiophene]-5,5''-diyl]	—	—	1.30	7.0	8.9 (2J), 9.64 (3J)	30
	PCDTBT: poly[[<i>N</i> -9''-hepta-decanyl-2,7-carbazole- <i>alt</i> -5,5-(4',7'-di-2-thienyl-2',1',3',5''-benzothiadiazole)]	-5.5	-3.6	1.88	6.33	7.0	84 and 45
	PBDTTT-CF: poly[4,8-bis-substituted-benzo[1,2- <i>b</i> :4,5- <i>b</i> 0]dithiophene-2,6-diyl- <i>alt</i> -4-substituted-thieno[3,4- <i>b</i>]thiophene-2,6-diyl]-derived polymer	-5.22	-3.45	1.6	7.73	—	34
	PBDTTT-E: poly[4,8-bis-substituted-benzo[1,2- <i>b</i> :4,5- <i>b</i> 0]dithiophene-2,6-diyl- <i>alt</i> -4-substituted-thieno[3,4- <i>b</i>]thiophene-2,6-diyl]-derived polymer	-5.01	-3.24	1.6	5.15	—	34
	PBDTTT-C: poly[4,8-bis-substituted-benzo[1,2- <i>b</i> :4,5- <i>b</i> 0]dithiophene-2,6-diyl- <i>alt</i> -4-substituted-thieno[3,4- <i>b</i>]thiophene-2,6-diyl]-derived polymer	-5.12	-3.35	1.6	6.58	—	34

that have optimal energy levels (HOMOs and LUMOs), near-infrared or infrared bandgaps, high carrier mobility, and good film morphology for large open circuit voltage, efficient light absorption for high current density, and high fill factor which are still lacking in triple or even quadruple junction polymer solar cells.

3.4. Interconnecting layer materials between subcells

Most materials used as interconnecting layers between subcells in multijunction polymer solar cells have been successfully incorporated either as interfacial layers (*i.e.* transport layers) or

collecting electrodes in single BHJ solar cells. Typical electron transport layers (ETLs) are ZnO,^{84,88} TiO₂/TiO_x,^{89–91} Nb₂O₅,^{92,93} and Cs₂CO₃,⁹⁴ while the commonly used hole transport layers (HTLs) are PEDOT:PSS,^{95,96} MoO₃,^{97–99} WO₃,¹⁰⁰ V₂O₅,¹⁰¹ NiO¹⁰² and NiAc.¹⁰³ When used as collecting electrodes (*e.g.*, ITO), these materials function to efficiently collect the photogenerated carriers. In addition to the role of charge transport and collection, these materials also serve to smoothen the electrode surface, provide transparency, act as optical spacers thus enhancing the internal optical electric field of the active layer,¹⁰⁴ and protect the active layer during electrode deposition. Typical interfacial layers studied in single junction BHJ devices include

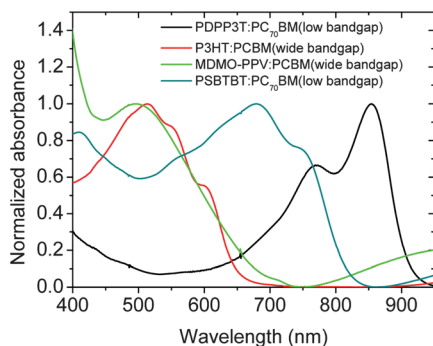


Fig. 10 Normalized absorption spectra of representative wide bandgap (P3HT and MDMO-PPV) and low bandgap (PSBTBT and PDPP3T) polymers blended with fullerene derivatives.

metal-oxides,^{84,93,105} doped metal-oxides,⁵⁴ cross-linkable charge-carrier selective materials,^{106–108} conjugated semiconducting electrolytes,^{109–111} self-assembled functional molecules,¹¹² and graphene.¹¹³ Intermediate layer materials in multijunction polymer solar cells are required to be optically transparent, function as an effective charge recombination site for electrons and holes,¹¹⁴ connect the subcells electrically through Ohmic contact and have physical robustness to protect underlying subcells when depositing top subcells.⁴⁰ Failure in satisfying these conditions is likely to result in an absorption loss in the back subcell and/or a loss in overall V_{oc} and J_{sc} , depending on the configuration of the multijunction cells. Fortunately, many challenges related to interfacial layers have been very well solved as evidenced in the high performance double and triple junction solar cells that have been recently reported.^{29,30,115}

3.4.1. Charge transfer processes at the interconnecting layer. To further shed light on the phenomenon of observed V_{oc} reduction or S-shaped $J-V$ curve due to inefficient interconnecting layers of both electron transport layer (ETL) and hole transport layer (HTL) in multijunction PSCs, our own group studied the energetic barrier formation at typical interconnecting layers by depositing Nb_2O_5 , ZnO, and TiO_2 on top of PCBM and PEDOT:PSS on top of polymer. As illustrated schematically in Fig. 11, electron transport from PCBM to ETL in the

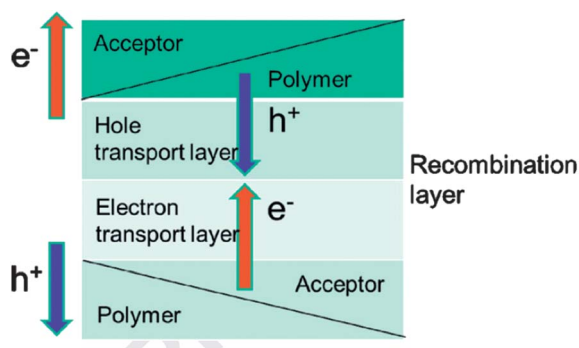


Fig. 11 Schematic diagram illustrating the role of interfacial layers. Reproduced with permission from ref. 20.

bottom subcell and hole transport from the conjugated polymer to HTL in the top subcell should provide efficient carrier recombination with no/minimal resistive or potential loss. Any imbalance of charge transfer, which can be caused by potential barrier formation at PCBM–electron transport layer interfaces, will lead to S-shaped $J-V$ curves with lower V_{oc} and poor fill factor in multijunction solar cells. This problem is not only limited to the multijunction structure but also has been observed in single junction organic solar cells, particularly in inverted architectures.^{90,91,116,117} Jasieniak *et al.* encountered such S-shaped $J-V$ curve behavior at the MoO_x /P3HT:PC₆₁BM interface in single junction polymer solar cells even at elevated annealing temperatures.¹¹⁸

The intermediate layer interfaces for Kelvin probe measurements were prepared by dropping one on top of the other, which covered the partial surface region and formed a step. Fig. 12a shows an AFM topography image of the PCBM– Nb_2O_5 interface. Nb_2O_5 is in the form of nanoparticles and its film thickness is ~ 12 – 14 nm. Fig. 12b shows a surface potential image of the Nb_2O_5 –PCBM interface, in which blue is for Nb_2O_5 and red is for PCBM. The physical height and surface potential (contact potential difference/CPD) profile *vs.* the lateral distance at the interface is shown in Fig. 12c. The Nb_2O_5 side showed a higher surface potential than PCBM. A green line separating the blue and red regions was probably originated from the inter-diffusion and inter-mixing of the two materials. Nb_2O_5 showed an energy barrier of ~ 0.2 eV for electron transfer from PCBM to Nb_2O_5 .

Fig. 12d shows the AFM surface topography image of the PCBM–ZnO interface. The interface was prepared by a similar method to that for the PCBM– Nb_2O_5 sample discussed above. The step is ~ 60 – 70 nm thick. Coating ZnO onto the PCBM surface did not destroy the underlying PCBM layer. Fig. 12e shows the surface potential across the PCBM–ZnO interface. The blue region on the left represents ZnO, while the red region on the right represents PCBM. Again the green line between the blue and red can be attributed to inter-diffusion of ZnO and PCBM. ZnO exhibited an energy barrier of ~ 0.12 V that can make it difficult for electron transport from PCBM to ZnO. Fig. 12f shows the height and surface potential profile *versus* the lateral distance across the interface. Although ZnO thicknesses are different, as is seen from the several peaks and valleys, the surface potential profile seems to be constant, which indicates that the roughness and thickness variation has no effects on the surface potential. The ZnO–PCBM interface exhibited a smaller energy barrier for electron transport than that (~ 0.2 eV) at the Nb_2O_5 –PCBM interface.²¹

Fig. 12g presents an AFM surface topography image of the PCBM– TiO_x interface. The PCBM– TiO_x interface samples were prepared with the same method as the above for Nb_2O_5 –PCBM and ZnO–PCBM interfaces. The deposition of TiO_x formed a clear step that is about 85–90 nm thick. There is no obvious damage to the PCBM layer after drop casting TiO_x . Fig. 12h shows the surface potential across the PCBM– TiO_x interface. In contrast to the Nb_2O_5 –PCBM and ZnO–PCBM interfaces where PCBM exhibits red and the metal oxides exhibit blue, both the PCBM and TiO_x sides exhibit the same green color. Fig. 12i

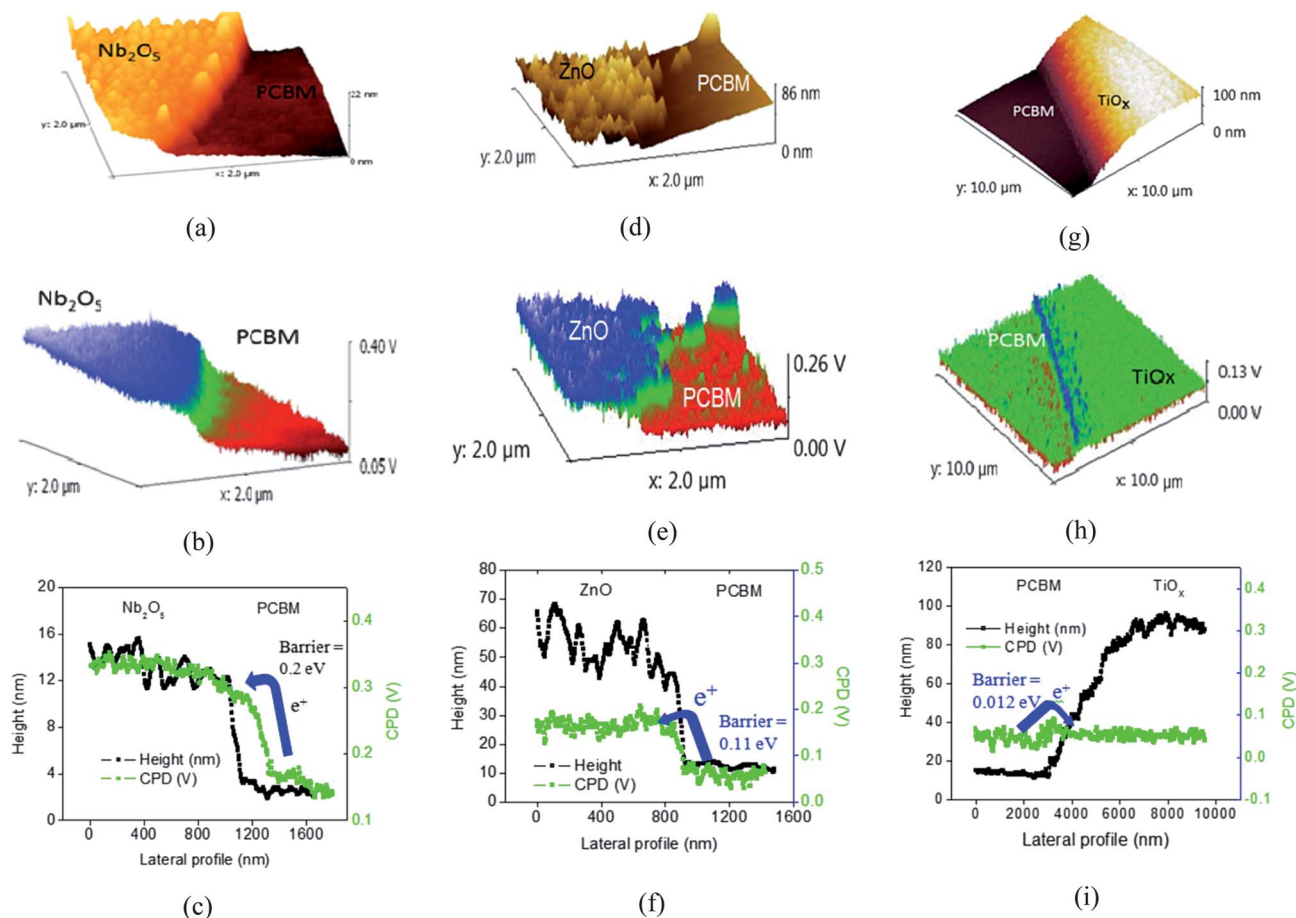


Fig. 12 Interface topography images of (a) PCBM–Nb₂O₅, (d) PCBM–ZnO, and (g) PCBM–TiO_x. Interface surface potential images of (b) PCBM–Nb₂O₅, (e) PCBM–ZnO, and (h) PCBM–TiO_x; the height and contact potential difference across the interfaces of (c) PCBM–Nb₂O₅, (f) PCBM–ZnO, and (i) PCBM–TiO_x. Reproduced with permission from ref. 21.

shows that TiO_x has a slightly different (~ 0.012 V) surface potential from the PCBM, indicating a tiny energy barrier for electron transfer from PCBM to TiO_x.²¹

In addition to the energy barriers for charge transfer from PCBM to various metal oxides, carrier mobilities and film thicknesses are also important factors that need to be considered. To further compare electron transfer from PCBM to various metal oxides, inverted polymer solar cells utilizing Nb₂O₅, ZnO, and TiO₂ as electron transport layers were prepared by our own group. The J - V characteristics of the Nb₂O₅-based device, as shown in Fig. 13, are poor owing to the higher work function of Nb₂O₅. Kelvin probe measurements showed the work function of Nb₂O₅ to be -3.8 eV which is higher than PCBM LUMO (-4.3 eV), causing an energy barrier for electron transfer from PCBM to Nb₂O₅. A similar study addressing the relationship between the cell performance and the Nb₂O₅ layer thickness of an inverted organic solar cell was reported by Wiranwetchayan *et al.*⁹³ Their result showed that the thinner Nb₂O₅ (10 nm) layer yielded the highest efficiency, suggesting that electron transfer occurs *via* tunnelling from PCBM to Nb₂O₅.⁹³ The requirement for tunneling is possibly the reason that the S-shaped J - V curve and lower V_{oc} are observed in Fig. 13. Improved J - V curves and higher V_{oc} were exhibited by

ZnO and TiO₂ based devices that could be attributed to the favorable energy level between PCBM LUMO and their conduction band, leading to a reduced energy barrier for electron transfer from PCBM to ZnO or TiO₂ as discussed above. Even though ZnO showed a slightly higher energy barrier than TiO₂, the highest current density was obtained by the ZnO based device possibly due to its highest electron mobility. This also led to the highest FF exhibited by ZnO based devices with the lowest series resistance.

Fig. 14a shows an AFM surface topography image of MDMO-PPV on top of the PEDOT-PSS layer, showing a clear interface formation between PEDOT:PSS and MDMO-PPV. The MDMO-PPV side (left) appears to be smoother than PEDOT-PSS on the right side. Fig. 14b shows a Kelvin probe force microscopy (KFM) surface potential image at the PEDOT:PSS-MDMO:PPV interface with a distinct separation between the two materials. A green striped region observed at the interface can possibly be caused by the inter-diffusion of PEDOT:PSS and MDMO-PPV into each other. Fig. 14c shows the physical height and surface potential variation profile across the PEDOT:PSS-MDMO:PPV interface. MDMO-PPV exhibits a surface potential that is ~ 0.14 eV lower than PEDOT:PSS. The lower surface potential in the MDMO-PPV side will support an energetically favorable hole

transport from itself to PEDOT:PSS. In addition, there are several peaks showing a significant thickness variation in the PEDOT:PSS side, however, their surface potential profile was quite flat. This suggested that the surface potential shows little dependence on the thickness. Similarly, the surface potential of the MDMO-PPV layer also exhibits no dependence on the film thickness although the thickness varies from 15 to 35 nm. This is consistent with the results observed for the PCBM–metal oxide interfaces discussed above.

3.4.2. New interconnecting materials. High annealing temperatures can be used to induce crystallinity in widely used metal-oxides; however, this cannot be performed on metal-oxides that are used as interconnecting layers in multijunction polymer solar cells. The high temperatures necessary to form crystalline lattice structures in metal-oxides are detrimental to active layers or plastic substrates. In addition, UV treatment has been commonly performed on metal-oxides to improve the device performance by producing an Ohmic contact at the interconnecting layers. However, there is a concern that UV illumination will harm the conjugated polymers in the active layers. Therefore, new materials or surface modifiers can be used as interconnecting layers to provide effective electron selectivity, hole-blocking, and modification of the work-function of ITO electrodes in inverted solar cells.

Kang *et al.* reported a 6.3% PCE using a non-conjugated polyelectrolyte (NPE) without using UV illumination in inverted polymer solar cells.¹¹⁹ The ITO work-function was drastically reduced by NPEs such as amines (polyethyleneimine – PEI) to 4.0 eV and protonated amines (polyallylamine – PAA) to 4.2 eV. Fig. 15 shows the chemical structures of these two NPEs: PEI and PAA. The chemical processes are also shown to occur when these NPEs are in aqueous solution and subsequently deposited on ITO.

Fig. 15a shows that NPE undergoes cationic characteristics which means that the functional amines of NPE can be partially protonated by accepting protons (H^+) that dissociate from water. When aqueous solutions of NPEs are subsequently deposited on the typically rough ITO surface as shown in Fig. 15b, electrostatic self-assembly occurs in which the protonated amines of the NPE undergo strong electrostatic

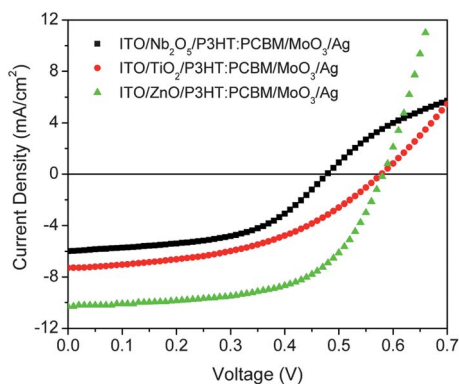


Fig. 13 J - V characteristics of the inverted organic solar cell utilizing Nb_2O_5 , ZnO , and TiO_2 as electron transport layers.

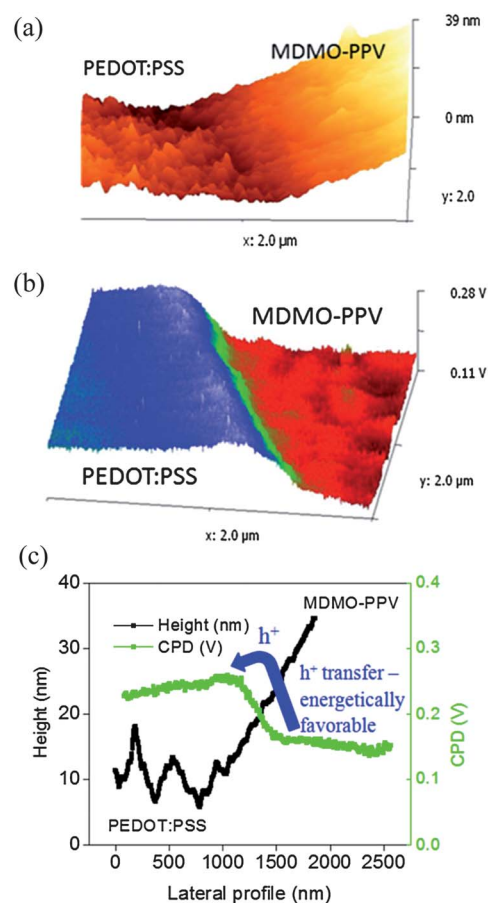


Fig. 14 (a) AFM surface topography images of PEDOT:PSS and MDMO-PPV layers and their interfaces; (b) KFM CPD images of the MDMO-PPV and PEDOT:PSS layers and their interfaces; and (c) surface topography and CPD diagram versus lateral profile across the MDMO-PPV/PEDOT:PSS interface. Reproduced with permission from ref. 21.

interaction with the negatively charged oxygen ion on the ITO surface. As depicted in Fig. 15c, a strong dipole is formed between NPE and ITO with the surface dipole moment pointing toward NPE. This dipole formation caused a downward vacuum level shift and consequently shifting of the work function of ITO. As shown in Fig. 16, an Ohmic contact can be established between the LUMO energy level of $PC_{70}BM$ and the ITO/PEI or ITO/PAA cathodes. Therefore, the use of NPEs eliminated the need for UV illumination in PEI as illustrated in the J - V curves shown in Fig. 17.

Zhou *et al.* reported work function modification of various materials such as ITO, ZnO , fluorine-doped tin dioxide (FTO), Au, Ag, Al, PEDOT:PSS and graphene by coating 10 nm thick polyethyleneimine ethoxylated (PEIE) and branched polyethyleneimine (PEI).¹²⁰ PEIE has a bandgap of 6.2 eV and may function as an insulator to block electron transport. However, electron injection can still occur *via* tunneling or thermionic injection if this layer is ultrathin (less than 10 nm). The authors found that neutral amine rather than the protonated one was more probably responsible for the work function shift. An ITO/PEIE/P3HT:IC₆₀BA/MoO₃/Ag device yielded a PCE of 5.95%. PEIE was later used as all-organic PEDOT:PSS/PEIE

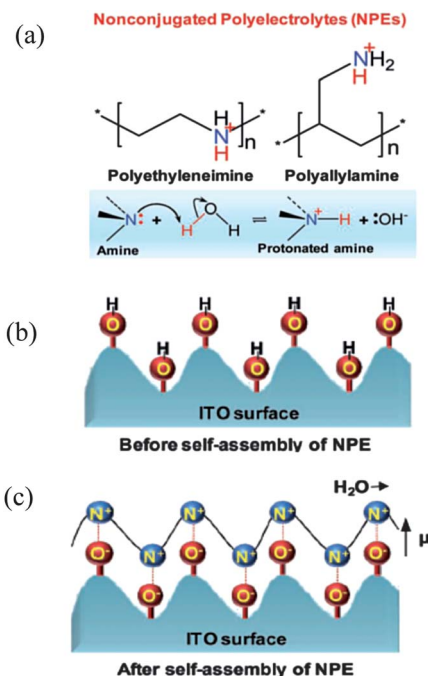


Fig. 15 Schematic illustration of (a) the chemical structure of two NPEs and the chemical processes of NPE in aqueous solution, (b) aqueous NPE deposition on the ITO surface before NPE self-assembly and (c) aqueous NPE deposition on the ITO surface after NPE self-assembly. Reproduced with permission from ref. 119.

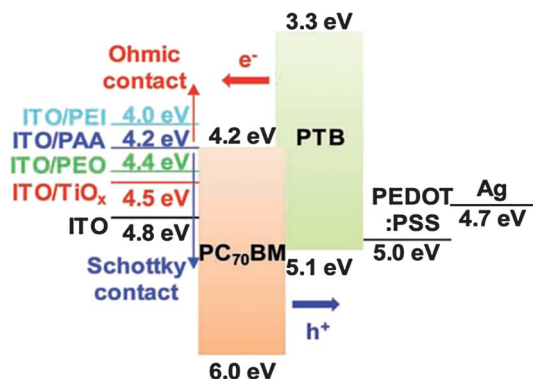


Fig. 16 Energy level diagram of an inverted polymer solar cell illustrating the cathode electrical contact with the LUMO level of PC₇₀BM. Reprinted with permission from ref. 119.

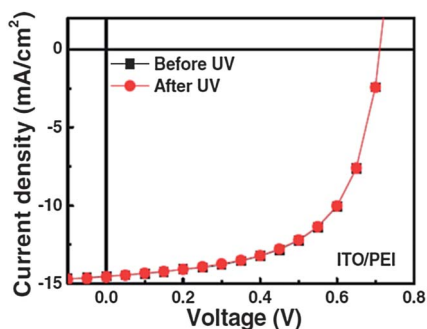


Fig. 17 UV independence of inverted PSCs incorporating the ITO/PEI cathode. Reprinted with permission from ref. 119.

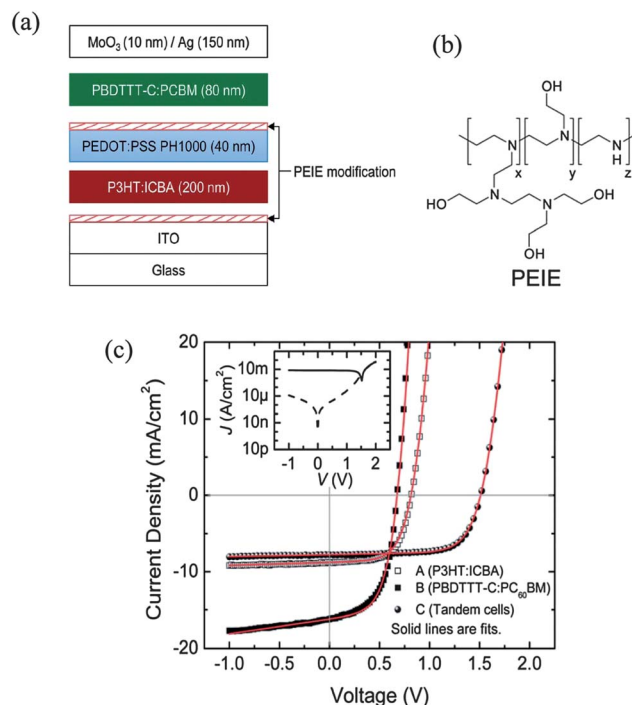


Fig. 18 (a) Double junction PSC device structure (b) chemical structure of the surface modifier-PEIE (c) corresponding J - V behaviour. Reprinted with permission from ref. 46.

interconnecting layer in a double junction solar cell comprising P3HT:IC₆₀BA and PBDTTT-C:PC₆₀BM photoactive layers. Fig. 18 shows the (a) device structure, (b) chemical structure of PEIE and (c) J - V curves of the PEDOT:PSS/PEIE interconnecting layer double junction polymer solar cells. The double junction cells were demonstrated with an efficiency of 8.2%, a J_{sc} of 7.7 mA cm⁻², V_{oc} of 1.50 V and FF of 0.72. The work function of PEIE modified PEDOT:PSS (PH1000) decreased from 4.9 eV to 3.6 eV. The PEIE modified PEDOT:PSS (PH1000) work function changed from 4.9 eV to 3.6 eV and no S-shaped J - V curves were observed indicating no requirement of UV illumination. In addition, the V_{oc} of the double junction cell (1.50 V) is almost the sum of the V_{oc} of individual subcells (0.83 V and 0.68 V), which suggested well matched energy levels at the interconnecting layers.

Other new intermediate layer materials such as graphene oxides and their composites have not been discussed here because Ameri *et al.* have reviewed them in their very recent work.³¹

4. Efficiency evolution in triple junction solar cells

In this section we will focus on the experimental results of triple junction devices because double junction based devices have been very well reviewed by Ameri *et al.* recently.³¹

In 2007, Gilot *et al.* reported a triple junction polymer solar cell prepared using two different material systems.¹⁰⁴ In one device, they used MDMO-PPV as both the light absorber and

donor in the front, middle and back cells. In the other device, MDMO-PPV was used in the front and middle cells, while P3HT in the back cells. ZnO and neutral pH PEDOT dispersion (Orgacon, batch 5541073, pH = 7, 1.2 wt%, Agfa Gevaert NV) were used as electron and hole transport layers, respectively. PCBM was used as an acceptor in each subcell. The subcell active layer thicknesses were increased from the front to back device, which allowed sufficient light to transmit to the middle and back cells for current matching. Fig. 19 shows the current density–voltage curves of the front, middle, back, and their combined triple junction cells with UV treatment.

Table 3 shows the list of the estimated and experimentally obtained (with and without UV treatment) open circuit voltages (V_{oc}) of triple junction polymer solar cells using ZnO/modified PEDOT as an intermediate layer. A non-Ohmic contact between the electron and hole transport layers (*e.g.* between ZnO and modified PEDOT in this case) can lead to a drop in V_{oc} and S-shaped J - V curves.¹⁰⁴ The Ohmic contact can be achieved by efficient doping in the electron and hole transport layers. PEDOT is deeply doped with PSS and ZnO can be doped by UV illumination, which was reported previously.¹⁰⁴ As shown in Table 3, the V_{oc} of the triple junction solar cells was increased from 1.40 to 1.92 V for MDMO-PPV/MDMO-PPV/MDMO-PPV and from 1.71 to 2.19 V for MDMO-PPV/MDMO-PPV/P3HT devices after the UV treatment.

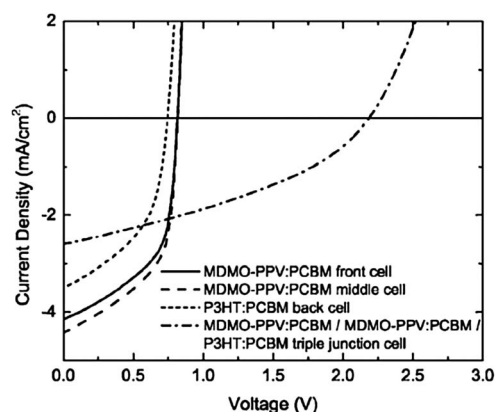


Fig. 19 Current density–voltage (J - V) curves for the front, middle, back, and their combined triple junction cells with UV treatment. Reproduced with permission from ref. 104.

Table 3 Estimated and experimentally obtained (with and without UV treatment) open circuit voltage (V_{oc}) of triple junction polymer solar cells using ZnO/modified PEDOT as an intermediate layer. Reproduced with permission from ref. 104

Front cell (45 nm)	Middle cell (65 nm)	Back cell (85 nm)	UV	V_{oc} (V)	V_{est} (V)
MDMO-PPV	MDMO-PPV	MDMO-PPV	No	1.40	2.46
			Yes	1.92	
MDMO-PPV	MDMO-PPV	P3HT	No	1.71	2.39
			Yes	2.19	

In 2009, Zhao *et al.* reported a triple junction polymer solar cell with identical P3HT and PCBM composites as the active layers in each subcell and highly transparent Al (1 nm)/MoO₃ (15 nm) as the intermediate layer.¹²¹ Fig. 20a and b show the device structure of triple junction P3HT:PCBM polymer solar cells and J - V curves of single, double and triple junction solar cells under simulated solar irradiation of 100 mW cm⁻². ITO was used as the bottom electrode and Al as the top electrode. The single junction first (front, active layer thickness = 70 nm), second (middle, active layer thickness = 85 nm), and third (back, active layer thickness = 50 nm) cells exhibited an efficiency of 1.94, 2.64, and 1.76% respectively. The double junction devices made of the bottom two subcells (70/85 nm) showed an efficiency of 2.19% with V_{oc} = 1.19 V, J_{sc} = 3.71 mA cm⁻² and FF = 0.496, while the triple junction cells made of all three subcells (70/85/50 nm) exhibited a η of 2.03% with V_{oc} = 1.73 V, J_{sc} = 2.41 mA cm⁻² and FF = 0.484. Although the triple junction cells did not show higher efficiencies than single junction cells, the V_{oc} is 1.73 V that is almost the sum of three single junction subcells with an individual subcell V_{oc} at \sim 0.62 V. This work showed that the Al/MoO₃ can serve as a high transparency, efficient protective, and structurally smooth intermediate layer, which can be further applied in triple junction devices with a combination of polymers having complementary absorption spectra.¹²¹ A minor disadvantage would be the vacuum based deposition of Al and MoO₃ with a base pressure of 2.0×10^{-4} Pa.

Then in 2013, Li *et al.* from the Janssen group reported a high performance triple junction polymer solar cell with an efficiency of up to 9.64%.³⁰ They used PCDTBT:PC₇₀BM as the

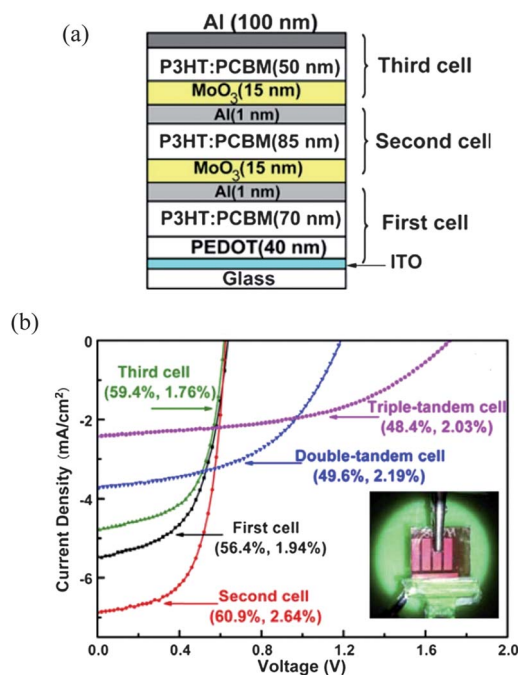


Fig. 20 (a) Device structure of triple junction P3HT:PCBM polymer solar cells and (b) J - V curves of single, double and triple junction solar cells under simulated solar irradiation of 100 mW cm⁻². Reproduced with permission from ref. 121.

active layer in the front cell, and PMDPP3T:PC₆₀BM as the active layer in the middle and back cells. Fig. 21a shows the triple junction solar cell device structure, where ZnO was used as the electron transport layer and pH neutral PEDOT:PSS as the hole transport layer was used as the intermediate recombination layer between subcells. The normal PEDOT:PSS coated ITO substrate was used as a bottom electrode to collect holes and LiF/Al as a top electrode to collect electrons. Fig. 21b shows the polymer absorption spectra. Polymer chemical structures are shown in Table 2. PCDTBT has a bandgap (E_g) of 1.8 eV and absorption mainly in the 350–650 nm wavelength range, while PMDPP3T's bandgap is 1.3 eV with the absorption band in the range of 600–950 nm. These absorption spectra are highly complementary. However, due to the current match

requirement, the lower photocurrent generated in the large bandgap PCDTBT limited the thickness of the low bandgap PMDPP3T. Therefore, the authors split the low bandgap PMDPP3T layer into two junctions in order to sufficiently harvest the photons in the low bandgap polymer.

Based on the dependence of predicted triple junction solar cell efficiency on the subcell thickness, they chose 125, 95, and 215 nm for the front, middle and back subcells respectively. The purpose for the back cell being thicker than the middle cell was to transmit the light from the middle to the back cell to ensure that they each harvest the same amount of photons for current matching because the same polymer was used in these two junctions. The authors conducted electrical–optical simulation on the double and triple junction structures where the PMDPP3T:PC₆₀BM was separated into two junctions. They found that the triple junction cells could lead to a higher device efficiency (9.2%) compared to that (8.46%) of the double junction cell. Fig. 21c shows the J - V curves of the front, middle, back cells and their combined triple junction cells (predicted and experimentally obtained). The triple junction cells showed a J_{sc} of 7.34 mA cm⁻², a V_{oc} of 2.09 V, a FF of 0.63, and a final efficiency (η) of 9.64%, showing an improved performance than that of double junction cells ($J_{sc} = 9.58$ mA cm⁻², $V_{oc} = 1.49$ V, FF = 0.62 and $\eta = 8.9%$). The reduced J_{sc} in triple junction cells was overcompensated by the significantly higher V_{oc} .

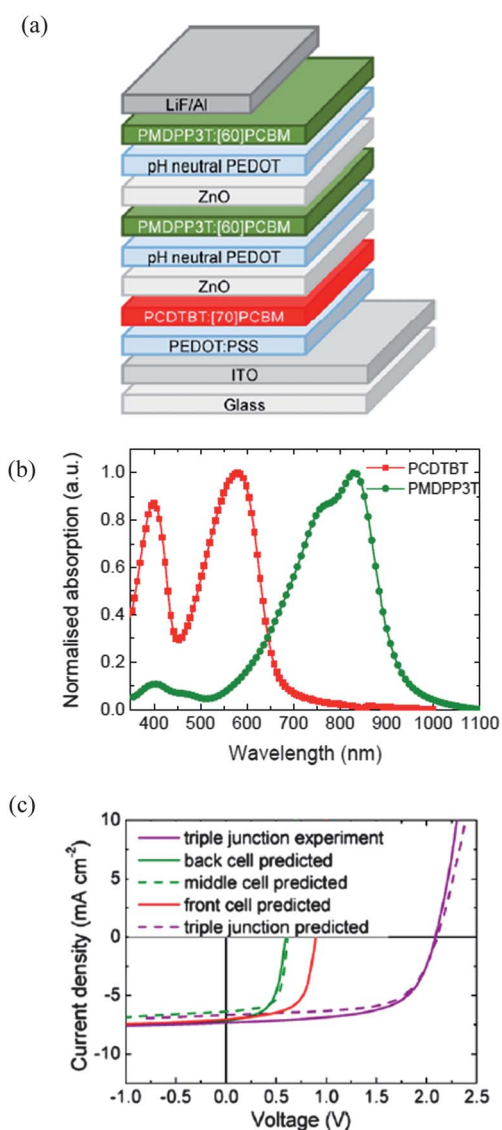


Fig. 21 (a) Chemical structures and (b) UV-Vis-NIR absorption spectra of PCDTBT and PMDPP3T, (c) triple junction solar cells using PCDTBT:PC₇₀BM in the front cell and PMDPP3T:PC₆₀BM in the middle and back cells, and (d) J - V curves of the front, middle, back and their combined triple junction cells (predicted and experimentally obtained). Reproduced with permission from ref. 30.

5. Conclusion and outlook

Recent reports showed that 11.1% single junction, 10.6% double junction and 9.64% triple junction polymer solar cells have been achieved.^{29,30,115} Single junction polymer solar cells will continue to advance in efficiency improvement despite their limitation due to the thermalization loss and energy loss required for exciton dissociation. The multijunction structure with its inherent potential to circumvent these limitations and losses of the single junction architecture will offer attractive benefits for achieving higher efficiency. Previous calculations by others and our own group have showed that double junction solar cells can potentially achieve an efficiency above 15%.^{3,20,122} However in the III-V group inorganic solar cells, the triple and quadruple junction solar cells have achieved an efficiency above 40%.^{123,124} Recent results for triple junction polymer cells from the Janssen group demonstrated a high possibility of using triple junction polymer cells to further increase the device efficiency. In addition, the experimentally obtained polymer triple junction solar cell efficiencies have been significantly increased as shown in Fig. 22. Based on the calculated predictions, the triple junction polymer solar cells are expected to significantly increase the cell efficiency and will attract extensive attention as future research focus and direction. Tremendous efforts have been made to synthesize various bandgap polymers to capture a wider band of the solar spectrum in multijunction polymer solar cells. To significantly increase light harvesting by adding more subcells into a multijunction structure, it is necessary to design and synthesize polymers with efficient absorption and bandgap into infrared regions as shown in Fig. 2 and 3. However, polymers or their combinations that can fully utilize

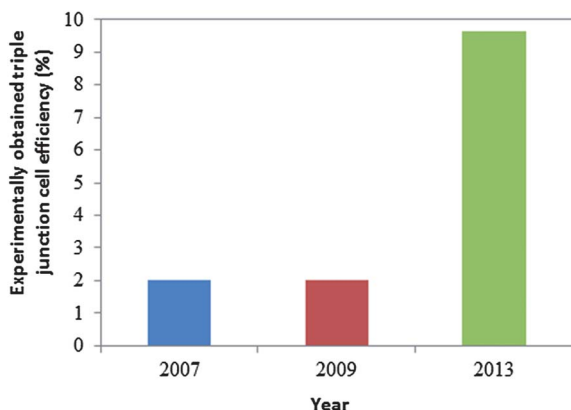


Fig. 22 Experimentally obtained polymer triple junction solar cell efficiency evolution. The efficiency for the year 2007 is a rough value.

the near infrared regions are still in infancy. Developments in the intermediate layer, donor, and acceptor materials are critical to maximize the organic solar cell efficiency. Different interconnecting layers with suitable transparency, mechanical and electrical behavior have been reported in the literature. It is expected that new interconnecting layer materials for superior performance without the need for vacuum processing will become available in the future. In addition, as new donor polymers and acceptor materials with effectively optical, electrical and reliably stable characteristics are being developed for single and double junction cells, these materials will likely find applications in triple junction devices, which will push up the efficiency further to realize potential low-cost and large-scale commercial viability.

Acknowledgements

We acknowledge the financial support from the US NSF CAREER award (ECCS-0950731), NASA EPSCoR (NNX13AD31A), National Science Foundation/EPSCoR Grant no. 0903804, and South Dakota Board of Regent CRGP. M. Wang acknowledges the National Natural Science Foundation of China (no. 11274307) for financial support. S. Y. acknowledges the financial support from the National Natural Science Foundation of China (nos. 90921013, 21132007) and the Fundamental Research Funds for the Central Universities (WK2060140005).

Notes and references

- 1 A. R. Jha, *Solar Cell Technology and Applications*, Taylor & Francis Group LLC, Boca Raton, 2010.
- 2 J. Nelson, *Mater. Today*, 2011, **14**, 462–470.
- 3 M. Siddiki, J. Li, D. Galipeau and Q. Qiao, *Energy Environ. Sci.*, 2010, **3**, 867–883.
- 4 G. F. Brown and J. Wu, *Laser Photonics Rev.*, 2009, **3**, 394–405.
- 5 G. Li, R. Zhu and Y. Yang, *Nat. Photonics*, 2012, **6**, 153–161.
- 6 Y. Xia, K. Sun and J. Ouyang, *Energy Environ. Sci.*, 2012, **5**, 5325–5332.
- 7 H. Zhang and J. Ouyang, *Appl. Phys. Lett.*, 2010, **97**, 063509.
- 8 J. J. Dittmer, W. U. Huynh and A. Paul Alivisatos, *Science*, 2002, **295**, 2425.
- 9 C. J. Brabec, S. Gowrisanker, J. J. M. Halls, D. Laird, S. Jia and S. P. Williams, *Adv. Mater.*, 2010, **22**, 3839–3856.
- 10 C. W. Tang, *Appl. Phys. Lett.*, 1986, **48**, 183–185.
- 11 J. J. M. Halls, C. A. Walsh, N. C. Greenham, E. A. Marseglia, R. H. Friend, S. C. Moratti and A. B. Holmes, *Nature*, 1995, **376**, 498–500.
- 12 G. Yu, J. Gao, J. C. Hummelen, F. Wudl and A. J. Heeger, *Science*, 1995, **270**, 1789–1791.
- 13 W. Ma, C. Yang, X. Gong, K. Lee and A. J. Heeger, *Adv. Funct. Mater.*, 2005, **15**, 1617–1622.
- 14 G. Li, V. Shrotriya, J. Huang, Y. Yao, T. Moriarty, K. Emery and Y. Yang, *Nat. Mater.*, 2005, **4**, 864–868.
- 15 W. Chen, T. Xu, F. He, W. Wang, C. Wang, J. Strzalka, Y. Liu, J. Wen, D. J. Miller, J. Chen, K. Hong, L. Yu and S. B. Darling, *Nano Lett.*, 2011, **11**, 3707–3713.
- 16 W. Chen, M. P. Nikiforov and S. B. Darling, *Energy Environ. Sci.*, 2012, **5**, 8045–8074.
- 17 A. Hadipour, B. de Boer, J. Wildeman, F. B. Kooistra, J. C. Hummelen, M. G. R. Turbiez, M. M. Wienk, R. A. J. Janssen and P. W. M. Blom, *Adv. Funct. Mater.*, 2006, **16**, 1897–1903.
- 18 D. Chen, A. Nakahara, D. Wei, D. Nordlund and T. P. Russell, *Nano Lett.*, 2010, **11**, 561–567.
- 19 Y. Xie, Y. Bao, J. Du, C. Jiang and Q. Qiao, *Phys. Chem. Chem. Phys.*, 2012, **14**, 10168–10177.
- 20 M. K. Siddiki, S. Venkatesan, M. Wang and Q. Qiao, *Sol. Energy Mater. Sol. Cells*, 2013, **108**, 225–229.
- 21 M. K. Siddiki, S. Venkatesan, D. Galipeau and Q. Qiao, *ACS Appl. Mater. Interfaces*, 2013, **5**, 1279–1286.
- 22 A. J. Breeze, Z. Schlesinger, S. A. Carter and P. J. Brock, *Phys. Rev. B: Condens. Matter Mater. Phys.*, 2001, **64**, 125205.
- 23 P. A. van Hal, M. M. Wienk, J. M. Kroon, W. J. H. Verhees, L. H. Slooff, W. J. H. van Gennip, P. Jonkheijm and R. A. J. Janssen, *Adv. Mater.*, 2003, **15**, 118–121.
- 24 P. Vanlaeke, A. Swinnen, I. Haeldermans, G. Vanhoyland, T. Aernouts, D. Cheyns, C. Deibel, J. D'Haen, P. Heremans, J. Poortmans and J. V. Manca, *Sol. Energy Mater. Sol. Cells*, 2006, **90**, 2150–2158.
- 25 M. T. Dang, L. Hirsch and G. Wantz, *Adv. Mater.*, 2011, **23**, 3597–3602.
- 26 J. C. Bijleveld, A. P. Zoombelt, S. G. J. Mathijssen, M. M. Wienk, M. Turbiez, D. M. d. Leeuw and R. A. J. Janssen, *J. Am. Chem. Soc.*, 2009, **131**, 16616–16617.
- 27 J. Hou, H.-Y. Chen, S. Zhang, G. Li and Y. Yang, *J. Am. Chem. Soc.*, 2008, **130**, 16144–16145.
- 28 F. B. Kooistra, J. Knol, F. Kastenberg, L. M. Popescu, W. J. H. Verhees, J. M. Kroon and J. C. Hummelen, *Org. Lett.*, 2007, **9**, 551–554.
- 29 J. You, L. Dou, K. Yoshimura, T. Kato, K. Ohya, T. Moriarty, K. Emery, C.-C. Chen, J. Gao and G. Li, *Nat. Commun.*, 2013, **4**, 1446.
- 30 W. Li, A. Furlan, K. H. Hendriks, M. M. Wienk and R. A. J. Janssen, *J. Am. Chem. Soc.*, 2013, **135**, 5529–5532.
- 31 T. Ameri, N. Li and C. J. Brabec, *Energy Environ. Sci.*, 2013, **6**, 2390–2413.

- 32 J. You, L. Dou, Z. Hong, G. Li and Y. Yang, *Prog. Polym. Sci.*, 2013, DOI: 10.1016/j.progpolymsci.2013.04.005.
- 33 M. C. Scharber, D. Wuhlbacher, M. Koppe, P. Denk, C. Waldauf, A. J. Heeger and C. L. Brabec, *Adv. Mater.*, 2006, **18**, 789–794.
- 34 H.-Y. Chen, J. Hou, S. Zhang, Y. Liang, G. Yang, Y. Yang, L. Yu, Y. Wu and G. Li, *Nat. Photonics*, 2009, **3**, 649–653.
- 35 S. H. Park, A. Roy, S. Beaupre, S. Cho, N. Coates, J. S. Moon, D. Moses, M. Leclerc, K. Lee and A. J. Heeger, *Nat. Photonics*, 2009, **3**, 297–302.
- 36 P. Peumans, A. Yakimov and S. R. Forrest, *J. Appl. Phys.*, 2003, **93**, 3693–3723.
- 37 W. L. Ma, C. Y. Yang, X. Gong, K. Lee and A. J. Heeger, *Adv. Funct. Mater.*, 2005, **15**, 1617–1622.
- 38 Y. Liang, Y. Wu, D. Feng, S.-T. Tsai, H.-J. Son, G. Li and L. Yu, *J. Am. Chem. Soc.*, 2009, **131**, 56–57.
- 39 A. Hadipour, B. de Boer and P. W. M. Blom, *Org. Electron.*, 2008, **9**, 617–624.
- 40 J. Yang, R. Zhu, Z. Hong, Y. He, A. Kumar, Y. Li and Y. Yang, *Adv. Mater.*, 2011, **23**, 3465–3470.
- 41 L. Dou, J. You, J. Yang, C.-C. Chen, Y. He, S. Murase, T. Moriarty, K. Emery, G. Li and Y. Yang, *Nat. Photonics*, 2012, 180–185.
- 42 J. Gilot, M. M. Wienk and R. A. J. Janssen, *Adv. Energy Mater.*, 2010, **22**, E67–E71.
- 43 S. Sista, M.-H. Park, Z. Hong, Y. Wu, J. Hou, W. L. Kwan, G. Li and Y. Yang, *Adv. Mater.*, 2010, **22**, 380–383.
- 44 J. Y. Kim, K. Lee, N. E. Coates, D. Moses, T.-Q. Nguyen, M. Dante and A. J. Heeger, *Science*, 2007, **317**, 222–225.
- 45 V. S. Gevaerts, A. Furlan, M. M. Wienk, M. Turbiez and R. A. J. Janssen, *Adv. Mater.*, 2012, 1–5.
- 46 Y. Zhou, C. Fuentes-Hernandez, J. W. Shim, T. M. Khan and B. Kippelen, *Energy Environ. Sci.*, 2012, **5**, 9827–9832.
- 47 P. Boland, K. Lee, J. Dean and G. Namkoong, *Sol. Energy Mater. Sol. Cells*, 2010, **94**, 2170–2175.
- 48 Y. Min Nam, J. Huh and W. H. Jo, *Sol. Energy Mater. Sol. Cells*, 2011, **95**, 1095–1101.
- 49 G. Namkoong, P. Boland, K. Lee and J. Dean, *J. Appl. Phys.*, 2010, **107**, 124515–124516.
- 50 B. Minnaert and P. Veelaert, *Materials*, 2012, **5**, 1933–1953.
- 51 G. Dennler, K. Forberich, T. Ameri, C. Waldauf, P. Denk, C. J. Brabec, K. Hingerl and A. J. Heeger, *J. Appl. Phys.*, 2007, **102**, 123109–123109-6.
- 52 J. Y. Kim, K. Lee, N. E. Coates, D. Moses, T. Q. Nguyen, M. Dante and A. J. Heeger, *Science*, 2007, **317**, 222–225.
- 53 M. M. Wienk, J. M. Kroon, W. J. H. Verhees, J. Knol, J. C. Hummelen, P. A. van Hal and R. A. J. Janssen, *Angew. Chem.*, 2003, **115**, 3493–3497.
- 54 M.-H. Park, J.-H. Li, A. Kumar, G. Li and Y. Yang, *Adv. Funct. Mater.*, 2009, **19**, 1241–1246.
- 55 Y. He, G. Zhao, B. Peng and Y. Li, *Adv. Funct. Mater.*, 2010, **20**, 3383–3389.
- 56 B. Kraabel, C. H. Lee, D. McBranch, D. Moses, N. S. Sariciftci and A. J. Heeger, *Chem. Phys. Lett.*, 1993, **213**, 389–394.
- 57 N. S. Sariciftci, L. Smilowitz, A. J. Heeger and F. Wudl, *Science*, 1992, **258**, 1474–1476.
- 58 N. S. Sariciftci, D. Braun, C. Zhang, V. I. Srdanov, A. J. Heeger, G. Stucky and F. Wudl, *Appl. Phys. Lett.*, 1993, **62**, 585–587.
- 59 Y. Yao, C. Shi, G. Li, V. Shrotriya, Q. Pei and Y. Yang, *Appl. Phys. Lett.*, 2006, **89**, 153507.
- 60 G. Zhao, Y. He and Y. Li, *Adv. Mater.*, 2010, **22**, 4355–4358.
- 61 Y. He, C. Chen, E. Richard, L. Dou, Y. Wu, G. Li and Y. Yang, *J. Mater. Chem.*, 2012, **22**, 13391–13394.
- 62 Y. He, H.-Y. Chen, G. Zhao, J. Hou and Y. Li, *Sol. Energy Mater. Sol. Cells*, 2011, **95**, 1762–1766.
- 63 Y. He, H.-Y. Chen, G. Zhao, J. Hou and Y. Li, *Sol. Energy Mater. Sol. Cells*, 2011, **95**, 899–903.
- 64 E. Ahmed, G. Ren, F. S. Kim, E. C. Hollenbeck and S. A. Jenekhe, *Chem. Mater.*, 2011, **23**, 4563–4577.
- 65 J. E. Anthony, *Chem. Mater.*, 2010, **23**, 583–590.
- 66 Z. Bao, A. Dodabalapur and A. J. Lovinger, *Appl. Phys. Lett.*, 1996, **69**, 4108–4110.
- 67 S. Müller, G. Fanchini, Y.-Y. Lin, C. Li, C.-W. Chen, W.-F. Su and M. Chhowalla, *J. Mater. Chem.*, 2008, **18**, 306–312.
- 68 A. L. Ayzner, D. D. Wanger, C. J. Tassone, S. H. Tolbert and B. J. Schwartz, *J. Phys. Chem. C*, 2008, **112**, 18711–18716.
- 69 T. Erb, U. Zhokhavets, G. Gobsch, S. Raleva, B. Stühn, P. Schilinsky, C. Waldauf and C. J. Brabec, *Adv. Funct. Mater.*, 2005, **15**, 1193–1196.
- 70 J. Y. Kim, S. H. Kim, H.-H. Lee, K. Lee, W. Ma, X. Gong and A. J. Heeger, *Adv. Mater.*, 2006, **18**, 572–576.
- 71 X. Hu, M. Shi, J. Chen, L. Zuo, L. Fu, Y. Liu and H. Chen, *Macromol. Rapid Commun.*, 2011, **32**, 506–511.
- 72 J. Hou, T. L. Chen, S. Zhang, L. Hou, S. Sista and Y. Yang, *Macromolecules*, 2009, **42**, 9217–9219.
- 73 S. Ko, E. Verploegen, S. Hong, R. Mondal, E. T. Hoke, M. F. Toney, M. D. McGehee and Z. Bao, *J. Am. Chem. Soc.*, 2011, 16722–16725.
- 74 A. Dhanabalan, J. K. J. van Duren, P. A. van Hal, J. L. J. van Dongen and R. A. J. Janssen, *Adv. Funct. Mater.*, 2001, **11**, 255–262.
- 75 D. Mühlbacher, M. Scharber, M. Morana, Z. Zhu, D. Waller, R. Gaudiana and C. Brabec, *Adv. Mater.*, 2006, **18**, 2884–2889.
- 76 J. F. Peet, J. F. Kim, N. F. Coates, W. F. Ma, D. F. Moses, A. F. Heeger and G. C. Bazan, *Nature*, 2007, **6**, 497–500.
- 77 N. Blouin, A. Michaud and M. Leclerc, *Adv. Mater.*, 2007, **19**, 2295–2300.
- 78 J. C. Bijleveld, V. S. Gevaerts, D. D. Nuzzo, M. Turbiez, S. G. J. Mathijssen, D. M. d. Leeuw, M. M. Wienk and R. A. J. Janssen, *Adv. Energy Mater.*, 2010, **22**, E242–E246.
- 79 H. Bronstein, Z. Chen, R. S. Ashraf, W. Zhang, J. Du, J. R. Durrant, P. Shakya Tuladhar, K. Song, S. E. Watkins, Y. Geerts, M. M. Wienk, R. A. J. Janssen, T. Anthopoulos, H. Sirringhaus, M. Heeney and I. McCulloch, *J. Am. Chem. Soc.*, 2011, **133**, 3272–3275.
- 80 Y. Liang, Y. Wu, D. Feng, S.-T. Tsai, H.-J. Son, G. Li and L. Yu, *J. Am. Chem. Soc.*, 2008, **131**, 56–57.
- 81 L. Dou, J. Gao, E. Richard, J. You, C.-C. Chen, K. C. Cha, Y. He, G. Li and Y. Yang, *J. Am. Chem. Soc.*, 2012, **134**, 10071–10079.

- 82 Z. Yi, X. Sun, Y. Zhao, Y. Guo, X. Chen, J. Qin, G. Yu and Y. Liu, *Chem. Mater.*, 2012, **24**, 4350–4356.
- 83 M. M. Wienk, M. G. R. Turbiez, M. P. Struijk, M. Fonrodona and R. A. J. Janssen, *Appl. Phys. Lett.*, 2006, **88**, 153511.
- 84 Y. Sun, J. H. Seo, C. J. Takacs, J. Seifert and A. J. Heeger, *Adv. Mater.*, 2011, **23**, 1679–1683.
- 85 Y. Liang, Z. Xu, J. Xia, S.-T. Tsai, Y. Wu, G. Li, C. Ray and L. Yu, *Adv. Mater.*, 2010, **22**, E135–E138.
- 86 P. Maharjan, Q. Chen, L. Zhang, O. Adebajo, N. Adhikari, S. Venkatesan, P. Adhikary, B. Vaagensmith and Q. Qiao, *Phys. Chem. Chem. Phys.*, 2013, 6856–6863.
- 87 W. Zhang, J. Smith, S. E. Watkins, R. Gysel, M. McGehee, A. Salleo, J. Kirkpatrick, S. Ashraf, T. Anthopoulos, M. Heeney and I. McCulloch, *J. Am. Chem. Soc.*, 2010, **132**, 11437–11439.
- 88 A. K. K. Kyaw, X. W. Sun, C. Y. Jiang, G. Q. Lo, D. W. Zhao and D. L. Kwong, *Appl. Phys. Lett.*, 2008, **93**, 221107.
- 89 J. Li, S. Kim, S. Edington, J. Nedy, S. Cho, K. Lee, A. J. Heeger, M. C. Gupta and J. T. Yates, *Sol. Energy Mater. Sol. Cells*, 2011, **95**, 1123–1130.
- 90 C. S. Kim, S. S. Lee, E. D. Gomez, J. B. Kim and Y.-L. Loo, *Appl. Phys. Lett.*, 2009, **94**, 113302–113303.
- 91 H. Schmidt, K. Zilberberg, S. Schmale, H. Flugge, T. Riedl and W. Kowalsky, *Appl. Phys. Lett.*, 2010, **96**, 243305.
- 92 M. K. Siddiki, S. Venkatesan and Q. Qiao, *Phys. Chem. Chem. Phys.*, 2012, **14**, 4682–4686.
- 93 O. Wiranwetchayan, Z. Liang, Q. Zhang, G. Cao and P. Singjai, *Mater. Sci. Appl.*, 2011, 1697–1701.
- 94 H.-H. Liao, L.-M. Chen, Z. Xu, G. Li and Y. Yang, *Appl. Phys. Lett.*, 2008, **92**, 173303.
- 95 S.-I. Na, G. Wang, S.-S. Kim, T.-W. Kim, S.-H. Oh, B.-K. Yu, T. Lee and D.-Y. Kim, *J. Mater. Chem.*, 2009, **19**, 9045–9053.
- 96 Y. Xia and J. Ouyang, *J. Mater. Chem.*, 2011, **21**, 4927–4936.
- 97 Y. Sun, C. J. Takacs, S. R. Cowan, J. H. Seo, X. Gong, A. Roy and A. J. Heeger, *Adv. Mater.*, 2011, **23**, 2226–2230.
- 98 L. Cattin, F. Dahou, Y. Lare, M. Morsli, R. Tricot, S. Houari, A. Mokrani, K. Jondo, A. Khelil, K. Napo and J. C. Bernede, *J. Appl. Phys.*, 2009, **105**, 034507.
- 99 T. Stubhan, T. Ameri, M. Salinas, J. Krantz, F. Machui, M. Halik and C. J. Brabec, *Appl. Phys. Lett.*, 2011, **98**, 253308.
- 100 C. Tao, S. Ruan, G. Xie, X. Kong, L. Shen, F. Meng, C. Liu, X. Zhang, W. Dong and W. Chen, *Appl. Phys. Lett.*, 2009, **94**, 043311–043313.
- 101 J. Wu, J. Hou, Y. Cheng, Z. Xie and L. Wang, *Semicond. Sci. Technol.*, 2007, **22**, 824.
- 102 P.-C. Yang, J.-Y. Sun, S.-Y. Ma, Y.-M. Shen, Y.-H. Lin, C.-P. Chen and C.-F. Lin, *Sol. Energy Mater. Sol. Cells*, 2011, 351–356.
- 103 Z. a. Tan, W. Zhang, D. Qian, C. Cui, Q. Xu, L. Li, S. Li and Y. Li, *Phys. Chem. Chem. Phys.*, 2012, **14**, 14217–14223.
- 104 J. Gilot, M. M. Wienk and R. A. J. Janssen, *Appl. Phys. Lett.*, 2007, **90**, 1435121–1435123.
- 105 D. H. Wang, S. H. Im, H. K. Lee, O. O. Park and J. H. Park, *J. Phys. Chem. C*, 2009, **113**, 17268–17273.
- 106 F. Huang, Y.-J. Cheng, Y. Zhang, M. S. Liu and A. K. Y. Jen, *J. Mater. Chem.*, 2008, **18**, 4495–4509.
- 107 Y. Sun, X. Gong, B. B. Y. Hsu, H.-L. Yip, A. K. Y. Jen and A. J. Heeger, *Appl. Phys. Lett.*, 2010, **97**, 193310–193313.
- 108 Y. Sun, S.-C. Chien, H.-L. Yip, Y. Zhang, K.-S. Chen, D. F. Zeigler, F.-C. Chen, B. Lin and A. K. Y. Jen, *Chem. Mater.*, 2011, **23**, 5006–5015.
- 109 S.-H. Oh, S.-I. Na, J. Jo, B. Lim, D. Vak and D.-Y. Kim, *Adv. Funct. Mater.*, 2010, **20**, 1977–1983.
- 110 Y. Zhao, Z. Xie, C. Qin, Y. Qu, Y. Geng and L. Wang, *Sol. Energy Mater. Sol. Cells*, 2009, **93**, 604–608.
- 111 K. Yao, L. Chen, Y. Chen, F. Li and P. Wang, *J. Mater. Chem.*, 2011, **21**, 13780–13784.
- 112 H.-L. Yip, S. K. Hau, N. S. Baek, H. Ma and A. K. Y. Jen, *Adv. Mater.*, 2008, **20**, 2376–2382.
- 113 L. Sangchul, Y. Jun-Seok, J. Yongsung, C. Chunhum, K. Dong-Yu, N. Seok-In, L. Byoung Hun and L. Takhee, *Nanotechnology*, 2012, **23**, 344013.
- 114 C. Zhang, S. W. Tong, C. Jiang, E. T. Kang, D. S. H. Chan and C. Zhu, *Appl. Phys. Lett.*, 2008, **92**, 083310.
- 115 Z. He, C. Zhong, S. Su, M. Xu, H. Wu and Y. Cao, *Nat. Photonics*, 2012, **6**, 591–595.
- 116 T. Kuwabara, T. Nakayama, K. Uozumi, T. Yamaguchi and K. Takahashi, *Sol. Energy Mater. Sol. Cells*, 2008, **92**, 1476–1482.
- 117 R. Steim, S. A. Choulis, P. Schilinsky and C. J. Brabec, *Appl. Phys. Lett.*, 2008, **92**, 093303.
- 118 J. J. Jasieniak, J. Seifert, J. Jo, T. Mates and A. J. Heeger, *Adv. Funct. Mater.*, 2012, **22**, 2594–2605.
- 119 H. Kang, S. Hong, J. Lee and K. Lee, *Adv. Mater.*, 2012, **24**, 3005–3009.
- 120 Y. Zhou, C. Fuentes-Hernandez, J. Shim, J. Meyer, A. J. Giordano, H. Li, P. Winget, T. Papadopoulos, H. Cheun, J. Kim, M. Fenoll, A. Dindar, W. Haske, E. Najafabadi, T. M. Khan, H. Sojoudi, S. Barlow, S. Graham, J.-L. Brédas, S. R. Marder, A. Kahn and B. Kippelen, *Science*, 2012, **336**, 327–332.
- 121 D. W. Zhao, X. W. Sun, C. Y. Jiang, A. K. K. Kyaw, G. Q. Lo and D. L. Kwong, *IEEE Electron Device Lett.*, 2009, **30**, 490–492.
- 122 G. Dennler, M. C. Scharber, T. Ameri, P. Denk, K. Forberich, C. Waldauf and C. J. Brabec, *Adv. Mater.*, 2008, **20**, 579–583.
- 123 S. Philipps, W. Guter, E. Welsler, J. Schöne, M. Steiner, F. Dimroth and A. Bett, *Next Generation of Photovoltaics*, 2012, pp. 1–21.
- 124 Z. Alferov, V. Andreev and V. Rumyantsev, *High-Efficient Low-Cost Photovoltaics*, 2009, pp. 101–141.